Dmrt2 Orchestrates Neuronal Development in the Embryonic Cingulate Cortex: Unveiling Sex-Biased Vulnerabilities

Ana Bermejo-Santos, Rodrigo Torrillas-de la Cal, Miguel Rubio-García
and Esther Serrano-Saiz*

Centro Biología Molecular Severo Ochoa (CBM) – CSIC

Corresponding author: Esther Serrano-Saiz
Address: Centro Biología Molecular Severo Ochoa (CBM) – CSIC
Email: eserrano@cbm.csic.es

ABSTRACT

Sexual differences are prevalent in the brain. DMRT family of transcription factors (TF) has been postulated as an important determinant of sex differences. Up to now, the role of DMRTs in the brain has been focused on the DMA subfamily. Here, we show an unprecedented role for *Dmrt2* in regulating the proliferation and neuronal development of cortical neurons in mice. *Dmrt2* expression is observed in deep-layer neurons of the cingulate cortex (CgCx) throughout development. Downregulation of *Dmrt2* mRNA in the CgCx primordium results in premature cell cycle exit of embryonic progenitors and subsequent reduction in cortical plate cellular density at later developmental stages.

Dmrt2 is expressed at higher levels in male embryos during early development, potentially explaining their increased vulnerability to *Dmrt2* depletion. As development progresses, *Dmrt2* expression is maintained in deeper-layer neurons, where this TF controls distinct terminal processes, including migration, axonal targeting, and neuronal-specific gene expression.

Our findings suggest a potential mechanistic link between the function of a *Dmrt* family member and sex-specific susceptibility to neurological disorders. This study expands our understanding of *Dmrt* gene function in the brain and provides insights into the molecular basis of sexual differences in neurodevelopmental processes.

INTRODUCTION

Sex differences are prominent in nearly every neuropsychiatric and neurodevelopmental disorder, influencing the age of onset, prevalence, symptomatology, diagnosis, and therapeutic response[1,2]. The genetic factors involved in the sexual differentiation of the brain could underlie the sexual bias and etiology of psychiatric disorders. The *doublesex and mab-3-related transcription factor* (*Dmrts*) gene family stands out for its evolutionary conservation as key regulators of sex determination and differentiation [3-5]. The family is defined by the region that mediates DNA binding, the DM domain, which is in all *Dmrts* [6]. A DMRT subgroup has an additional domain, the DMA domain of unknown function. *Dmrts* have been extensively studied in the sexual differentiation of invertebrate nervous systems (NS) and have been implicated in the control of cell death, terminal identity differentiation, and synaptic connectivity to, ultimately, generate sex-specific circuit configurations [7,8]. However, we currently lack a full understanding of the role of *Dmrt* genes in sexual differentiation within mammalian NS.

In mammals, a role in the NS has only been addressed for the subfamily of DMA-*Dmrts* (including *Dmrt3*, *Dmrt4,* and *Dmrt5*) (reviewed in[9]). Work in vertebrate embryos (mice and *Xenopus Laevis*) shows that, depending on the cellular context, DMA-*Dmrts* are involved in maintaining the proliferative capacity of neural progenitor cells in the mouse medial telencephalon [10,11] or neuronal differentiation processes [12-14].

Besides the DMA subfamily, other family members, including *Dmrt2*, are also expressed in the mouse brain, but no neuronal function has been attributed to them yet. The cingulate cortex (CgCx) primordium is one of the earliest regions where *Dmrt2* is detected. *Dmrt2* has been previously identified as expressed in postmitotic cingulate corticothalamic projection neurons (CThPNs), where it is proposed to exert late developmental functions, such as synaptic targeting and maturation[15]. *Dmrt2* functions have been exclusively described outside the NS, where it plays important roles in cell type differentiation, particularly in somite development. Here, *Dmrt2* regulates dermomyotomal and myotomal transcription factors, including PAX3 and MYF5, required to initiate skeletal muscle formation[16,17]. In addition, *Dmrt2* is a key player in chondrocyte differentiation during bone formation. *Dmrt2* acts as a *Sox9*-inducible gene that promotes the transition from a proliferative to a more differentiated hypertrophic stage[18].

Although little is known about the function of *DMRT2* in the human brain, several studies have shown that deletion or duplication of the short arm of chromosome 9, where *DMRT1*, *DMRT2*, and *DMRT3* are located, is associated with several mental disorders

or intellectual disabilities. These include developmental delay and craniofacial anomalies, autism spectrum disorder [19,20], and obsessive-compulsive disorder [21,22]. More specifically, *DMRT2* has been postulated as a risk factor for obsessive-compulsive disorder [23]. While no studies have specifically identified the neuronal function of DMRT2, one report conducted in human neuroblastoma cells shows that DMRT2 regulates both the proliferation rate and the progression of tumor growth[24]. However, the mechanisms by which *DMRT2* may induce or influence these processes *in vivo* have not yet been described.

In this study, we have analyzed the role of *Dmrt2* in the development of the mouse cingulate cortex, a region critical for emotional processing, executive function, and social behavior. By comparing male and female mouse embryos, we studied a novel link between *Dmrt2* function and the sexual differentiation of the mammalian NS. First, we thoroughly examined *Dmrt2* expression in the mouse CgCx at embryonic and postnatal time points in males and females. We asked whether there are sexual and developmental differences between *Dmrt2* transcriptional variants predicted by the NCBI genome browser (NCBI Gene ID: 226049). Then, we performed a functional analysis by downregulating, with interference RNA (iRNA), or overexpressing *Dmrt2* through *in utero* electroporations (IUE). We compared transcriptional profiles of male and female embryos and the general progression of proliferation, migration, and differentiation of cingulate cortical neurons. Our results provide valuable insights into developmental neurobiology and sex-based neuroscience by exploring the intersection of *Dmrt2* function, sex-specific development, and cortical formation.

RESULTS

Dmrt2 is expressed in mouse deep-layer cingulate cortical neurons

We analyzed the expression of *Dmrt2* by *in situ* hybridization (ISH) in male and female embryos (E) at E14.5 and E18.5, and postnatal (P) 7 (**Figure 1A-1D, Supplementary Figure 1A**) and adults P56 animals (**Supplementary Figure 1B**). We used a previously published riboprobe encompassing the coding RNA sequence [17] (**Figure 1E**).

By E14.5, *Dmrt2* is clearly detected in the cortical plate of the CgCx primordium in both sexes (**Figure 1A**). Already by E18.5, *Dmrt2* occupies the CgCx in its entire rostrocaudal axis (**Figure 1B**), excluding the somatosensory cortex. We look at P7, when migration is complete, to identify *Dmrt2* CgCx neurons through double immunofluorescence and ISH. We use TBR1 as a general marker of deeper layer VI[25] and CThPN identity [26] and SATB2 as a marker of upper callosal projection neurons (CPN) (layer II to VI, although expression in layer VI is dimmer) [27]. *Dmrt2*-labeling is strong in layer VI-TBR1+ cells

across the rostrocaudal length of the CgCx (**Figure 1C, c', d'**). An additional superficial cluster is detected in the anterior CgCx, where *Dmrt2* colocalizes with SATB2 in layer V CPN (**Figure 1C, c''**). At postnatal stages, a population of *Dmrt2*+ cells is clearly found in layer V, defined by CTIP2 [26] (**Figure 1C, d''**). In summary, *Dmrt2* is primarily expressed in cingulate, deeper CThPNs from mid-gestation embryos until postnatal animals and in a few scattered CPNs.

***Dmrt2.1* is expressed at higher levels in males during early cortical development**

The NCBI genome browser shows that the *Dmrt2* locus has three alternative transcript variants (Gene ID: 226049). According to predictions, *Dmrt2.2* and *Dmrt2.3* retain exon 4, which contains an alternative stop codon. Thus, *Dmrt2.2* is predicted to produce a shorter protein containing a longer 3'UTR than *Dmrt2.1* or *Dmrt2.3*. Both *Dmrt2.1* and *Dmrt2.2* sequences include the DM domain (located in exon 2, indicated in green in **Supplementary Figure 2A**). On the other hand, *Dmrt2.3.* mRNA will be transcribed from a cryptic transcription start site in exon 2, but its translation will commence from an alternative start site in exon 5. This protein product will lack the DM domain and share the 3'UTR with *Dmrt2.1* (**Supplementary Figure 2A**). Whether or not these variants are expressed in the mouse NS has never been addressed.

To test whether there is a sex-specific effect on *Dmrt2* expression levels, we performed real-time quantitative PCR (RT-qPCR) at E13.5, E14.5, E18.5, P7 and P56 stages. We included samples from antero-dorsal cortices containing the CgCx from male and female embryos (from E18 on, we excluded the hippocampus). One set of primers, designated "*Dmrt2.1"*, detects the *Dmrt2.1* variant specifically (**Figure 1E**). Another primer pair, "*Dmrt2.2/2.3*" detects *Dmrt2.2* and *Dmrt2.3* but does not distinguish them (**Supplementary Figure 2A**). At E13.5, *Dmrt2.1* is significantly more expressed in male embryos than in females (1,67 times more). This trend is clearly observed at E14.5 (p-value = 0.065); however, at later developmental stages, we no longer detect any sexual difference between the two sexes (**Figure 1F**). Only the *Dmrt2.1* variant shows a differential expression between male and female animals, while *Dmrt2.2/2.3* are similarly expressed in the two sexes at all developmental time points (**Supplementary Figure 2B**). Thus, we focus our study on *Dmrt2.1* from now on.

***Dmrt2* is required in post-mitotic neurons for migration and axon guidance**

Dmrt2 is robustly expressed at late developmental stages in post-mitotic neurons and maintained until adulthood (**Figure 1**, **Supplementary Figure 1A, 1B**). We analyzed the function of *Dmrt2* using a downregulation strategy through IUE using interference RNA. We electroporated a plasmid codifying for a short hairpin (sh) RNA, designated sh*Dmrt2*,

at E13.5 when deeper layer cortical neurons are born [28] (sh1 in **Figure 1E**). We confirmed that the sh*Dmrt2* induces *Dmrt2* downregulation by measuring *Dmrt2.1* mRNA levels by qRT-PCR of the ipsilateral cingulate cortex after 2 days of electroporation at E15.5. (**Supplementary Figure 3B**).

At E18.5, we analyzed the downregulation effect five days after IUE when the migration of deeper neurons should be mostly complete and axonal extension is taking place. We then compared these results with mock electroporated brains (see **Experimental Procedures** for details).

In mock electroporated animals at E18.5, GFP(+) cells populate homogeneously all layers of the CgCx and extend projections ipsilaterally towards the thalamus dorsally to the internal capsule, while a subset of axons crosses the midline through the corpus callosum (cc) (**Figure 2A, 2C; Supplementary Figure 3C, 3E**). In sh*Dmrt2* embryos, GFP(+) cells are also distributed along the CgCx, although they show several aberrant phenotypes (**Figure 2B, 2D**; **Supplementary Figure 3D, 3F; Table 1; Supplementary Table 1, 2**). First, we quantified the GFP(+) total fluorescence intensity (integrated density (IntDen)) of the cingulate cortical plate (CP) (leaving out the intermediate zone (IZ) and the ventricular and subventricular zones (VZ/SVZ)) (red dashed line in **Figure 2A-2D**). We found a 33% reduction in males (15% non-significant reduction of fluorescence intensity in females) (**Figure 2E**). Second, we analyzed the GFP(+) cell distribution in the four conditions. We selected a representative region of interest and divided it into 10 bins (red solid boxes in **Figures 2a'-d'**). We measured the fluorescence intensity (IntDen) within each individual bin. Bins 10-9 correspond to deeper layers just right above the cc, while bins 1-3 comprise the most external layers containing the newly generated neurons that had migrated the most. TBR1 highly expressing neurons (deeper layer VI) correspond roughly to intermediate bins 8-6 and layer V to bins 5-4. In mock embryos, most GFP(+) fluorescence accumulates in intermediate layers. However, in sh*Dmrt2* male embryos, bins closer to the cc show a significant increase in fluorescence at the expense of intermediate bins (**Figure 2F**). This phenotype is observed in both sexes but it is more exacerbated in females. In sh*Dmrt2* brains, we found GFP(+) cells stacked in the cc along the whole anterior-posterior axis of the CgCx (white arrowheads in **Figures 2b', d'; Supplementary Figure 3D, 3F**). By quantifying the total number of cells "misplaced" at the cc, we found that the effect is significantly higher in females (**Figure 3G; Table 1; Supplementary Table 1, 2**). In both sexes, those cells colocalize with TBR1 and CTIP2, but only some with SATB2 (**Supplementary Figure 3G**), suggesting migration defects. These cells are never found in mock animals. Third, we systematically observed that the VZ/SVZ is almost completely depleted of GFP(+) cells in the sh*Dmrt2* brains (**Figure 2a''-d''; Table 1; Supplementary Table 1, 2)**. The lack

of GFP(+) cells in the VZ/SVZ progenitor layer suggests a depletion in the progenitor pool due to the premature exit from the cell cycle in the sh*Dmrt2* electroporated cells. Eventually, post-mitotic cells will not be generated to populate the CP, which is what was observed (**Figure 2F**). Lastly, most GFP(+) cells extend projections to the thalamus, similar to mock brains. However, a subset of projections is misguided laterally, above the external capsule, instead of following the corticothalamic track. In the sh*Dmrt2* brains, this tract and the cc are de-fasciculated (**Fig 2a'''-d'''; Table 1; Supplementary Table 1, 2**). In summary, these results demonstrate that *Dmrt2* downregulation affects the neurogenesis and proper development of CgCx deeper neurons.

***Dmrt2* downregulation results in a more pronounced decrease of cingulate cortex neural precursors in male embryos**

The strong reduction of GFP(+) cells in the VZ/SVZ layer of sh*Dmrt2* brains at E18.5 suggests that *Dmrt2* downregulation could trigger the premature exit from the cell cycle in cingulate cortex progenitors. To analyze the progenitor layer, as well as early processes of neuronal migration, we look at two days after electroporation at E15.5 (**Figure 3)**. First, we analyzed the total cellular density of GFP(+) cells across the cingulate primordium (number of GFP(+) cells/μm^2). It is strongly reduced in sh*Dmrt2* males from 2.63±0.12 vs. 1.35±0.29 10^3 cells/μm^2. The effect is not significant in female embryos, although it follows a similar trend (2.30±0.35 vs 1.85±0.36 10^3 cells/μm^2) (**Figure 3E**). This phenotype is clearly appreciated in the images (**Figure 3A-3D**). Next, to identify whether *Dmrt2* is affecting neurogenesis or proliferation, we performed a series of quantifications of GFP(+) within three layers, each of them defined by different markers (**Supplementary Figure 4A**): the VZ, with mostly progenitor cells; the IZ, where cells are migrating and axons are growing; and the CP, where mature neurons migrate. In mock electroporated embryos, more than half of total GFP(+) cells are located at the VZ (59.84±4.04% in males and 45.68±8.59% in females) where apical progenitors reside (Ki67+) (**Figure 3F, Supplementary Figure 4A**). As cells differentiate, they migrate towards the IZ (dim TBR1) and the CP (high TBR1)[29]. 23.06±2.64% of GFP(+) cells are located in the IZ in males and 21.27±2.91% in females. The rest of the GFP(+) cells populate the CP (17.11±2.63% in males and 14.59±3.15% in females). Therefore, our quantification indicates no differences in the cellular distribution of electroporated cells between the sexes in mock animals (**Figure 3F**). This can be similarly observed when we represent the cellular density/layer (**Figure 3G**). Most of the GFP(+) cells are located in the VZ in both sexes (2.91±0.17 and 2.57±0.47 in males and females, respectively). Then, we compared the cellular distribution of GFP(+) in *Dmrt2* downregulation to mock

conditions. In sh*Dmrt2* embryos, there is a prominent decrease in the proportion of VZ-GFP(+) cells compared to mock embryos (**Figures 3F, 3G**). However, this reduction is only significant in males (59.84±4.04% in mock vs. 21.95±5.55% in sh*Dmrt2*. In females, there are 45.68±8.59% in mock vs. 32.88±11.44% in sh*Dmrt2*). Concomitantly, there is an increase in the proportion of IZ-GFP(+) cells, although it does not reach significant differences in any sex (23.06±2.64% in mock vs. 19.41±4.51% in sh*Dmrt2* in males; while in females, there is a 21.27±2.91% in mock vs. 22.46±1.30% in sh*Dmrt2*). Lastly, CP-GFP(+) cells show a slight decrease in their proportions (17.11±2.63% in mock vs. 9.76±3.32% in sh*Dmrt2* males, while there are 14.59±3.15% in mock vs. 11.92±2.58% sh*Dmrt2* females) (**Figure 3F**). Although these comparisons between mock and sh*Dmrt2* in the IZ and CP layers do not reach significant differences, they show a clear trend in their variation. The cellular density (**Figure 3G**) clearly shows the alteration of the GFP(+) development progression. In sh*Dmrt2*-treated embryos, GFP(+) cells accumulate in the IZ and do not reach the CP layer as expected if progenitors quickly exit the VZ.

At E15.5, *Dmrt2* is robustly detected in the CP by ISH, and we could not detect *Dmrt2* transcripts in the VZ/SVZ or the IZ (**Supplementary Figure 4B**). However, we confirmed that the phenotype observed in this study is specific to *Dmrt2* by electroporating a distinct sh*RNA* (sh2*,* **Figure 1E**) and obtaining similar results (**Supplementary Figure 4C**). Moreover, we took the opposite approach and overexpressed the canonical *Dmrt2.1* through IUE at E13.5 (oe*Dmrt2.1*). After two days from electroporation, at E15.5, the GFP(+) cellular distribution shows the opposite phenotype to the sh*Dmrt2* conditions: *Dmrt2.1* overexpression caused a strong decrease in CP-GFP(+) cells at the expense of an increase in the VZ-GFP(+) and IZ-GFP(+) cells (**Supplementary Figure 4E-4G**), indicating that *Dmrt2.1* overexpression caused an increase of progenitors´ proliferation. Altogether, *Dmrt2* downregulation is prominently affecting the VZ layer, depleting the progenitor pool, followed by an increase in cells at the IZ layer and a decrease in the CP. Moreover, *Dmrt2* downregulation affects male embryos more strongly than female embryos. The strong reduction of GFP(+) cells in the VZ suggests that *Dmrt2* is required to maintain progenitor cells in a proliferative state. When it is downregulated, progenitor cells exit prematurely the cell cycle. However, after they exit the cell cycle, GFP(+) cells tend to accumulate in the IZ and do not properly reach the CP. *Dmrt2.1* overexpression triggers the opposite effect and keeps progenitors in a proliferative state.

Loss of general neuronal identity of CgCx neurons upon *Dmrt2* depletion

Based on our anatomical analysis, *Dmrt2* downregulation affects the correct specification of cingulate neurons by controlling their migration and targeting. We asked whether

Dmrt2 could have a role in acquiring neuronal terminal identity. For this experiment, we performed an unbiased RNA-Seq from fluorescence-activated cell-sorted (FACS) electroporated cells. Like the previous experiment, embryos were electroporated at E13.5 into the CgCx primordium. At E18.5, FACSorted electroporated fluorescence cells were selected, and total mRNA was isolated and sent for sequencing (see **Experimental Procedures** for details).

The principal component analysis (PCA) showed that sh*Dmrt2*-treated embryos are clustered together, separate from mock embryos. Within sh*Dmrt2* samples, male and female embryos are mixed and do not segregate by sex, while mock samples are further clustered by sex (**Figure 4A**).

To proceed with the analysis, we selected Differentially Expressed Genes (DEGs) with an adjusted p-value (p-adj) < 0.05 and a Log2 Fold Change (FC) ≥ |1| (only genes that are at least two-fold up- or down-regulated) between four comparisons: mock male vs. mock female; sh*Dmrt2* male vs. sh*Dmrt2* female; sh*Dmrt2* male vs. mock male and, lastly, sh*Dmrt2* female vs. mock female (**Figure 4B**; **Supplementary Figure 5B; Supplementary Tables 3-5**). Overall, in the male-to-female comparisons, both in mock and sh*Dmrt2*, only a very reduced number of DEGs were retrieved (3 genes in mock: *Pf4* is downregulated and *Scml4* and *Serpina3n* are upregulated; 6 genes in sh*Dmrt2* comparisons: *Stk11*, *Npm3*, *Cd151* and *Mpst* are downregulated, while *Lhx6* and *Stac* are upregulated (**Supplementary Figure 5B**). However, when we compared sh*Dmrt2* vs. mock-treated cells in each sex, the differences in the number of DEGs were more pronounced. Interestingly, we retrieved 2.4 times more DEGs in female than male comparisons (**Figure 4B**).

Our initial analysis focused on *Dmrt2* expression levels. Surprisingly, in male cells, we observed that the sh*Dmrt2* treatment did not result in a statistically significant reduction of *Dmrt2* expression compared to the mock treatment (15.5% reduction; p-adj = 0.4524) (**Supplementary Figure 5C**; **Supplementary Table 4**). On the contrary, females show a 56.25% reduction (p-adj = 0.0216) (**Supplementary Table 3**). We then conducted a comparison between male and female datasets, which yielded 488 and 1163 DEGs, respectively, and found that approximately two-thirds of the DEGs identified in males were also present in the female dataset, indicating a substantial overlap in gene expression changes between sexes (**Venn diagram in Figure 4B; Supplementary Table 5**).

To comprehensively characterize the phenotype, we conducted a gene ontology (GO) study by Gene Set Enrichment Analysis (GSEA) on sh*Dmrt2* vs. mock DEGs. Only DEGs from female comparisons are shown in **Figure 4C-4F**. Although similar biological

processes are affected in both sexes, a few categories were specifically found in the male comparisons (**Supplementary Figure 5D, 5E**): *epithelium development*, *embryo development*, *animal organ morphogenesis*, *anatomical structure development* or *enzyme-linked receptor protein signaling pathway* (a few of these genes are: *Lama5, Cobl, Cd151, Aldh1a3, Tshz3, Met, Bmp6, Bmp2, Aplnr, Tie1, Robo4, Cldn5, Sox18, Zic1*, *Dok3*, *Hpgd, Lpxn, Apln, Htra3, Bmp2, Cldn5…*). Although all these genes show significant p values in female comparison, they do not meet the p-adj criteria. Most likely, the same processes are affected in both sexes but with differential magnitude (**Supplementary Table 4**).

On the female comparison GSEA, we selected 15 categories with Normalized Enrichment Scores (NES) > |2| (**Figure 4C, 4D**; **Supplementary Table 3**). The analysis of the most significant downregulated categories suggests that migration and neuronal functions are altered. Additionally, cell junction organization, calcium (Ca) and potassium (K) channel activity genes [Ca channel subunits (*Cacna1f*, *Cacng3*) and Ca binding proteins (*Cabp4*, *Cpne5, Rph3a*), K-channel subunits (*Kcns1*, *Kcnj2, Kcnj6, Kcng2*)], neurotransmitter pathway genes [serotonin transporter *Slc6a4*/*Sert* and glutamate receptors and interacting proteins *Grin2a, Grip2*], synaptic vesicle, pre and post-synapse activity [the transmembrane protein, such as *Ptchd1*, *Npas4* or *Prkcg/PKC-gamma*] show the highest reduction in expression in the female comparison.

The most significant GO terms among the up-regulated DEGs include immune response, cytokine production, cell cycle, cell chemotaxis, cell killing, extracellular space, and regulation of cell adhesion (**Figure 4E, 4F**). *Tumor necrosis factor (Tnf)* and several genes encoding TNF receptors (*Tnfrsf1b, Tnfrsf13b*…, etc.) or TNF-related proteins (*Tnfaip8*) are also upregulated. Interestingly, the TNF pathway has been involved in neurite outgrowth inhibition [30]. Genes involved in the secretion of extracellular matrix components are also upregulated (several matrix metallopeptidases or *Mmp* genes or collagens like *Col24a1,* for example) [31]. *Dmrt2* regulates (directly or indirectly) many genes that encode cell adhesion molecules (CAMs), such as cadherins, nectins, and netrins, that are required in the control of many neurodevelopmental aspects, including neural migration, axonal pathfinding, and wiring, along with synapse formation[32]. These processes regulate neurogenesis, cell migration, and axonal outgrowth and guidance[30-35]. Interestingly, many genes encoding chemokines and cytokines are among the most up-regulated genes [*Ccl5*, *Ccl12*, *Ccl9,* among others] and their receptors [*Ccr5* and *Cx3cr1*]. Canonical markers of microglia like *Cx3cr1 and Iba1* (also known as *Aif1*) show up in our list of DEGs. We discarded the possibility of microglia contamination in our

FACSorted cells because only electroporated ventricular progenitors carry the *pDsRed* plasmid.

Most *Dmrt2* neurons in the CgCx can be identified as TBR1-CThPN. However, *Dmrt2* does not regulate any of the TFs that have been previously characterized for cortical projection neurons subtype regulators, except for *Satb2* expression, which is reduced at approximately 50% of its level in mock conditions (log2FC = -0.97; p-adj = 0.00013), and *Ctip1* (also known as *Bcl11a*), which is moderately reduced by 28% (log2FC = -0,48; p-adj = 0.01). Notably, the expression of *Tbr2* (also known as *Eomes*) showed a 2-fold increase in *Dmrt2*-depleted neurons (log2FC = 1.07; p-adj = 1.45e-10). This substantial upregulation, coupled with a moderate rise in *Pax6* expression (log2FC = 0.73, p-adj = 0.00026) and increased levels of cell cycle-related genes (**Figure 4E**), indicates that neurons with reduced *Dmrt2* expression may retain characteristics of an immature state. In conclusion, the gene expression profile of cells with reduced *Dmrt2* levels reveals a complex pattern of transcriptional changes. Specifically, we observed a decrease in the expression of neuron-specific genes and an increase in non-neuronal gene expression. Most of the genes regulated by *Dmrt2* are functional effectors and not master regulators of cortical projection neuron identities. This transcriptional shift suggests that *Dmrt2* plays a crucial role in terminally defining the overall neuronal identity of CgCx neurons.

DISCUSSION

We have uncovered a novel function for the transcription factor *Dmrt2* in mouse cortical development. Specifically, we show an unprecedented function in the coordination of cingulate cortex neuronal differentiation. Our research deepens our understanding of the role of *Dmrt2*, going beyond its established peripheral functions. It also addresses a broader question regarding the interaction between genetic factors that regulate sexual differentiation and those that shape general brain development in mammals. Furthermore, we explored the conservation of *Dmrt* transcription factors in the sexual differentiation of the mammalian nervous system and identified sex-specific susceptibilities between male and female embryos upon *Dmrt2* downregulation.

Dmrt2.1 presents sexual differences in levels of expression during cingulate cortical development

Our results show that *Dmrt2* is highly enriched in post-mitotic CgCx neurons and expressed in deep-layer neurons across the entire rostrocaudal extension of the CgCx. Expression in this region is maintained from the early embryo until adulthood. This result, together with the previous report from Galazo *et al.* [15], situates *Dmrt2* in CThPNs. Our

analysis further shows that *Dmrt2* is not restricted to CThPNs, marked by TBR1, but a few scattered *Dmrt2* neurons colocalize with SATB2 in potentially callosal neurons. Additional tracing studies should be performed to confirm specific projections that might extend from *Dmrt2*-neurons to locations other than the thalamus.

At least three predicted *Dmrt2* variants will be transcribed from the *Dmrt2* locus (NCBI Gene ID: 226049) due to exon 4 retention, skipping, or transcription initiation. However, the only variant that showed statistically significant sexual differences was *Dmrt2.1,* while *Dmrt2.2* and *Dmrt2.3* did not show any differences at any time point. The lack of spatial resolution hampered our ability to discern whether the origin of the sexual difference comes from different levels in all *Dmrt2*-expressing cells or expression in distinct cell types. Single-cell RNA-Seq experiments comparing male and female embryos could shed light on this question, but unfortunately, such information is not available for the cingulate cortex.

Although no function has been assigned yet to *Dmrt2* alternative variants, future studies should be performed to uncover additional layers of regulation. DMRT2.1 and DMRT2.2 protein products differ in their C-terminal ends and could be controlling different target genes by binding distinct cofactors. These two variants also differ in their 3' untranslated regions where post-transcriptional regulation involving micro RNAs is crucial for controlling gene expression. Indeed, *in vitro* studies in neuroblastoma cell lines have shown that human *DMRT2* expression is regulated by *miR-16-5p* [24]. Additionally, post-transcriptional interactions between variants might exist. The potential product of *Dmrt2.3* bears no DNA binding domain and could act as a dominant negative. The human *DMRT2* locus is more complex, and many more variants are predicted to be transcribed (NCBI Gene ID: 10655 and [36]). However, a striking level of conservation in the regulatory logic between the human and murine loci makes our findings relevant for human studies. In humans, eleven predicted *DMRT2* mRNA isoforms involve exon 4 retention or skipping, a process that in mice produces *Dmrt2.1* and *Dmrt2.2.*, and alternative transcription initiation.

Interestingly, the sexual difference in *Dmrt2.1* levels was observed at E13.5 before the peak of testosterone secretion from the embryonic gonad had occurred yet [37]. Therefore, *Dmrt2.1* transcriptional differential levels might have an intrinsic chromosomal origin. DMRT TFs have been shown to control somatic morphological dimorphisms across phylogeny [4,5,7,38], which is usually ensured by their binary dimorphic expression. In the case of CgCx, we did not observe a dimorphic expression of *Dmrt2*; rather, we found quantitative differences between the sexes. Although subtle, these early differences in expression can lead to significant functional consequences, resulting in distinct

developmental outcomes between males and females at later stages. It is conceivable that as development progresses, we would have observed even more profound sexual functional differences in postnatal animals. Still, for those types of experiments, it is necessary to use more robust genetic models like conditional *Dmrt2* knock-outs where spatial and temporal manipulations could be performed, and rescue experiments could be done.

Dmrt2 controls general aspects of neuronal differentiation in post-mitotic neurons, including migration, axonal targeting, and gene expression

Dmrt2 has been previously described as an activator in the later stages of myoblast and chondrocyte differentiation. It is involved in the balance between self-renewal and differentiation [16,17]. Our research reveals that *Dmrt2* acts as a transcriptional regulator of the general terminal identity of deeper-layer neurons of the cingulate cortex.

We observed no changes in the expression of CThPN master regulators such as *Tbr1* or *Fog2*, suggesting that *Dmrt2* may operate downstream of this regulatory network. Galazo *et al*., proposed *Dmrt2* to be a late developmental gene that might be downstream of FOG2, although this was not tested specifically in the study [15]. Despite the limitations of our RNASeq in bulk approach, which precluded analysis of cell-specific processes, the observed reduction (although modest) in *Ctip1* and *Satb2* expression could indicate that one of the most affected neuron types are the deeper callosal neurons of layer V. It has been reported that in the absence of CTIP1 function, more subcortical projection neurons (SCPNs) are generated at the expense of both CThPNs and deeper CPNs[39]. SABT2 induces CPN identity and SCPN identity [40] with a limited role in regulating CThPN axons [26]. However, these TFs have been proposed to act in a context-dependent manner and have been mostly studied outside the CgCx, where layer and neuronal specification are not so well studied. It remains to be determined, with cellular resolution, the epistatic relationships between *Dmrt2* and them.

Numerous target genes involved in terminal neuronal functions have been identified to be regulated, directly or indirectly, by *Dmrt2*. The most overrepresented downregulated GSEA ontologies are fundamental for neuronal circuit assemblies and communication. Conversely, the upregulated-transcriptional landscape of *Dmrt2*-depleted cells reveals characteristics of an undifferentiated state (such as the upregulation of *Tbr2* and *Pax6*, or chemokine receptors, reported to be expressed in cortical progenitors [41]) and the inability to acquire the terminal identity of postmitotic projection neurons. This pattern of transcriptional changes suggests that *Dmrt2* may play a complex regulatory role in balancing neuronal specification processes during late-stage differentiation.

One of the most prominent phenotypes upon *Dmrt2* depletion is the impaired migration of deeper layer neurons and misguided projections and de-fasciculation. The RNA-seq *Dmrt2*-regulated targets corroborate the dysregulation of pathways governing these developmental processes: *Ctip1*, for which we found a modest reduction, is known to regulate these processes, and aberrant commissural projections are found in the CgCx of *Ctip1*^{Flox};*Emx*^{Cre} conditional knock-out mice [42]; or CAMs required in the control of many neurodevelopmental aspects, including neural migration, axonal pathfinding, and wiring, along with synapse formation are also affected [32,33,43]. Moreover, the prominent upregulation of chemokine-encoding genes and their receptors might directly affect neuronal migration defects. Neuronal expression of chemokines has been described before, and their downregulation in neurons has been proposed to influence many aspects of neuronal development, including differentiation, survival, and synaptic transmission [41,44-46].

Dmrt2 maintains the proliferative capacity of cortical progenitors, either through direct regulation or indirect mechanisms

Dmrt2 downregulation triggers the decrease in progenitor cells within the cingulate primordium´s ventricular zone. Conversely, *Dmrt2.1* overexpression produces the opposite outcome, increasing the ventricular zone proportion of cells at the expense of generating post-mitotic neurons. This result aligns with a previous report on human neuroblastoma cell lines where DMRT2 positively regulates the proliferation rate and progression of tumor growth [24]. ISH techniques employed in this study failed to detect *Dmrt2* mRNA expression in cortical progenitor cells. Furthermore, the absence of commercially available antibodies precludes direct examination of DMRT2 protein expression, which will eventually determine the TF function. We can envision two possibilities to explain the effect on progenitors: 1) a non-cell autonomous role for *Dmrt2* in the control of proliferation of progenitor cell cycle. Many genes we found misexpressed in *Dmrt2* downregulation cells encode for secreted molecules that might impact progenitors, or 2) *Dmrt2* expression levels are below the ISH detection threshold. The fact that we detect expression with RT-qPCR at E13.5 before we can observe any expression in the cingulate primordium through ISH, including in the CP where *Dmrt2* is clearly detected from E14.5, opens the possibility that *Dmrt2* is not detected in the VZ at any time point (not at E13.5 nor later) with this technique. Transcription factors often function at very low concentrations[47]. However, subtle changes in transcription factor levels can have significant functional consequences[48].

Other *Dmrts* genes, the DMA subfamily, have been previously described as having a role in the proliferation of cortical progenitor cells in mice. *Dmrt3* and *Dmrt5* are required to maintain the neural precursor cell proliferation in the medial pallio, which will generate the hippocampus [11]. This role is extensive to other species and has been extensively studied in the NS of *Drosophila,* where *doublesex* regulates neuroblast proliferation in a sex-specific manner [49-51]. Therefore, the interaction of *Dmrts* with the cell cycle becomes a recurring theme, and specific mechanistic details in neurons remain to be explored.

Dmrt2 may interact with intrinsic sex factors

By downregulating *Dmrt2* expression when deeper cortical neurons are born, we have uncovered potential sex differences in *Dmrt2*-dependent function.

Proliferation rates are not distinct between the sexes in mock embryos. However, when *Dmrt2* is depleted, latent sexual differences emerge, bearing males stronger phenotypes. *Dmrt2* downregulation unmasks sex-specific differences, prompting male progenitors to exit the cell cycle more rapidly than female ones and progress toward differentiation. This topic requires more research, but interestingly, glioblastoma, the most common brain tumor, presents sexual differences in the incidence and outcome. Such sex differences exist across all stages of life, indicating some independence from hormone action [52]. Although the precise mechanisms are unknown, a clinical correlation was found between cell cycle and integrin signaling.

The transcriptional profile analysis in late embryos reveals seemingly contradictory results, with female comparisons exhibiting higher numbers of DEGs than the male comparisons. Moreover, the lack of *Dmrt2* downregulation in male sorted cells suggests that mostly escapers - cells that have evaded *Dmrt2* depletion – are the ones that have completed their developmental trajectory, and, therefore, their transcriptional profile is more similar to mock-electroporated cells in males than in females. Similarly, migration and de-fasciculation defects are exacerbated in female brains. We interpret these results as a consequence of a stronger, earlier defect in male brains that results in a bigger depletion of post-mitotic cells. We could speculate that the result of these embryonic processes would impact behavior in postnatal animals, presumably with a poorer, or at least distinct, outcome in males than females. Additional studies are required to explore the genetic mechanisms that prime the susceptibility of male cells and whether cell cycle mechanisms present latent sexual differences.

DMRT2 and human intellectual disability

The CgCx is anatomically and functionally connected to a broad set of regions engaged in social information processing. Therefore, genetic mutations affecting its development could be associated with neurodevelopmental disorders such as cognitive disability, autism spectrum disorders, epilepsy, schizophrenia, and attention deficit hyperactivity disorder [53]. In this study, we report that *Dmrt2* regulates the proliferation and specification of deeper-layer CgCx projection neurons and that its effects are aggravated in male mice. The cingulate cortex has been postulated as one of the brain areas that shows sex differences in the elicited response to emotional stimuli[54] or anatomical features [55]. In rodents, sex differences have been found at the synaptic and connectivity levels [56,57]. Notably, it has been reported that males have a higher proportion of layer V neurons in the CgCx projecting to the prefrontal cortex than females [56]. Additional sex differences have been found at the level of synaptic plasticity in CgCx [57]. If similar mechanisms to those described in this paper are conserved, *DMRT2* could be involved in the development of the projection neurons of the human cingulate cortex. This could potentially explain males' increased vulnerability to neurodevelopmental disorders, providing a molecular basis for observed sex differences in these conditions. According to the Human Protein Atlas database, DMRT2 is present in the brain (https://www.proteinatlas.org/), but no other reports document its expression in the human brain.

DMRT2 is close to *DMRT1* and *DMRT3* in the short arm of chromosome 9. Deletions or duplications in that chromosomal region have been associated with intellectual disability and mental disorders [19,21,22,58]. *DMRT1* has been extensively studied in the human and mouse gonad [5], and no apparent neuronal expression has been reported. In mice, the DMA-DMRT *Dmrt3* is expressed in cortical progenitors [9], hindbrain [59], and spinal cord [60]. Potentially, its deletion could be related to intellectual disability in humans as well. However, this has not been proven yet, and no behavioral studies have been performed in mouse *Dmrt3* mutants or human patients with *DMRT3* mutations. Whether *DMRT2* mutations contribute to human intellectual disabilities through an aberrant development of the cingulate cortex will be of significant interest to investigate further.

EXPERIMENTAL METHODS

Animals and tissue preparation

Animals used in this study include male and female C57BL/6JRccHsd (ENVIGO) and C57BL/6J (The Jackson Laboratory) wildtype mice. Animals were housed and bred at the CBMSO animal facility and treated according to European Communities Council Directive 86/609/EEC regulating animal research. All procedures were approved by the Bioethics Subcommittee of Consejo Superior de Investigaciones Científicas (CSIC,

Madrid, Spain) and the Comunidad de Madrid (CAM) under the following protocol approval number (PROEX 286/19; RD 53/2013). The presence of a vaginal plug estimated embryonic day (E) 0.5 of pregnancy after overnight male mating.

For embryonic sex genotyping, tail tissue was collected and digested in 50 µl of $MgCl_2$-free PCR reaction buffer (10013-4104, Biotools) supplemented with 400 µg/ml proteinase K (3115879001, Roche) at 55°C with shaking for 1-3 hours (h), followed by heat-inactivation of the proteinase K at 95°C for 5 min. One microliter of a 1/10 dilution of each sample was added directly to a 25 µl PCR reaction. The protocol of genomic DNA amplification was adapted from McFarlane *et al.* [61]. The primers used were: *Sx*-Forward 5'-*GATGATTTGAGTGGAAATGTGAGGTA*-3' and *Sx*-Reverse 5'-*CTTATGTTTATAGGCATGCACCATGTA*-3' and the thermal protocol was: initial cycle of 5 minutes (min) at 94°C followed by 35 cycles of 45 seconds (s) at 94°C denaturalization, 30 s at 55°C annealing and 1 min at 72°C extension with a final extension step at 72°C for 10 min.

For staining, brains from embryos (E13.5, E14.5, E15.5, and E18.5) were fixed in 4% paraformaldehyde (PFA) (1.04005.1000, Merck) diluted in phosphate buffer (PBS 1X) for 2 h. Postnatal (P) 7 were fixed in 4% PFA for 4 h at room temperature (RT). Adult brains (P56) were fixed in 4% PFA overnight (o/n) at 4°C from animals previously perfused intracardially with sterile PBS 1X followed by 4% PFA. After fixation, brains were washed in PBS 1X several times, and cryoprotected in 15% sucrose (1.07651.1000, Merck)/PBS 1X. Lastly, they were embedded in 7.5% gelatin (G2625, Sigma)/15% sucrose (1.07651.1000, Merck)/PBS 1X and frozen at -80°C. Coronal cryostat sections were cut at 16 µm thickness.

For total RNA isolation, tissue was freshly collected from embryo and postnatal mouse brains and homogenized with 3 mm stainless steel Lysing beads (Alpha Nanotech, VWR) in diethyl pyrocarbonate (DEPC)-treated PBS (D5758, Sigma-Aldrich) for 1 min at 30 Hz with a TissueLyser (MM300, Retsch). Fresh or homogenized tissue was stored at -80º until use.

***In situ* hybridization (ISH)**

ISH was carried out as previously described by Di Meglio *et al.* [62]. Briefly, brain sections were incubated with 4% PFA for 10 min at 4°C. Then, prehybridization was performed at RT with hybridization buffer [50% deionized formamide (S4117, Millipore), SALTS 1X (Tris 10 mM, NaCl 200 mM, NaH_2PO4 5 mM, Na_2HPO_4 5 mM, EDTA 5 mM), Denhardt's 1X (D2532, Sigma), 10% dextran sulphate (4911, Sigma), tRNA 1 mg/ml (R6625, Sigma, Merck)] for 1 h in a humified chamber with 5X SSC [sodium citrate 750 mM, NaCl 75 mM] and 50% deionized formamide (S4117, Millipore). Tissue sections were incubated with the anti-sense digoxigenin-labeled (11277073910, Roche) probe (1:1000 in

hybridization buffer) o/n at 72°C. Following hybridization, the slides were washed in SSC 0.2X for 90 minutes at 72°C and then blocked in 2% blocking solution (11096176001, Roche) in MABT at pH 7.5 [maleic acid 100 mM, NaOH 200 mM, NaCl 200 mM, 0.1% Tween-20 (P1379, Sigma-Aldrich)] for 1 h at RT and then incubated o/n at 4°C with anti-digoxigenin-alkaline phosphatase antibody (11093274910, Roche) at 1:5000 diluted in MABT. After several washes, the alkaline phosphatase activity was developed using 3.5 µl/ml NBT (11383213001, Roche) and 1 µl/ml BCIP (11383221001, Roche) diluted in NTMT solution at pH 9.5 [Tris 100 mM, NaCl 100 mM, MgCl2 50 mM, 0.1% Tween-20 (P1379, Sigma-Aldrich)] for 20 h at RT. *Dmrt2* probe covers the whole gene except the first ATG and was kindly provided by Takahiko Sato[16] (see **Figure 1E**).

Fluorescent *in situ* hybridization (FISH)

The initial steps of hybridization were performed as described above. For detection, horseradish peroxidase-conjugated anti-digoxigenin antibody at 1:5000 (11207733910, Roche), TSA™ Plus Biotin System (NEL749A001KT, Perkin Elmer®), and 1:250 Streptavidin-Alexa 555 (S32355, Thermo Fisher) were used according to the manufacturer's instructions.

Immunofluorescent staining (IF)

IF was performed following standard protocols. Brain sections were washed with PBS 1X with 0.1% Triton™ X-100 (T9284, Sigma-Aldrich) (PBST) and blocked 1 h in blocking solution [PBST and 1% of bovine serum albumin (BSA) (A2153-100G, Sigma)]. The following primary antibodies diluted in a 1/10 blocking solution were incubated o/n at 4°C: chicken anti-GFP 1:1000 (ab13970, Abcam), rabbit anti-TBR1 1:300 (ab31940, Abcam), mouse anti-SABT2 1:50 (ab51502, Abcam), rat anti-CTIP2 1:500 (ab18465, Abcam), rabbit anti-Ki67 1:1000 (ab15580, Abcam) and sheep anti-TBR2 1:200 (AF6166, R&D System). In the case of TBR2, antigen retrieval was performed before primary antibody incubation (citrate buffer 10 mM, pH6, for 5 min at 110°C in a boiling chamber). Corresponding secondary antibodies were incubated at 1:1000 for 2 h at RT: goat anti-chicken-Alexa 488 (A11039, Thermo Fisher), donkey anti-mouse-Alexa 555 (A31570, Thermo Fisher), donkey anti-rabbit-Alexa 555 (A31572, Thermo Fisher), donkey anti-rabbit-Alexa 647 (A31573, Thermo Fisher), goat anti-rat-Alexa 555 (A21434, Thermo Fisher) and donkey anti-sheep-Cy3 (713-165-003, Jackson ImmunoResearch). Hoechst 33342 (H1399, Invitrogen™) was used for cell nuclei staining.

For double ISH or FISH and IF staining, ISH was carried out prior to IF as previously described [62].

Imaging

ISH chromogenic and IF images were obtained with a DMCTR5000 microscope equipped with DFC500 color and DFC350 FX monochrome cameras (Leica), respectively.

Tilescan mosaic images were acquired by SpinSR10 disk confocal system with an IX83 inverted microscope (Olympus) and reconstructed with CellSens Dimension 4.2.1 software (Olympus). All images were acquired using a 1024 × 1024 scan format with a 40x or 60x objective.

Integrated density (IntDen) was calculated using Fiji. For total IntDen, the IUE area was limited to the cingulate cortex and outlined manually. For cellular distribution, IntDen was measured in a defined area spanning from the cortical layer I to the corpus callosum (not included), subdivided into 10 equal bins.

Quantitative real-time PCR (qRT-PCR)

Total RNA was isolated using NZY Total RNA Isolation kit (MB13402, Nzytech) following the manufacturer's instructions. cDNA was obtained from 1 µg of total RNA with First-Strand cDNA Synthesis kit (27-9261-01, GE) in a 15 µl reaction volume. Quantitative real-time qRT-PCR was performed using GoTaq® qPCR Master Mix (A6002, Promega) following the protocol of the manufacturer in a CFX-384 Touch Real-Time PCR Detection System (Bio-Rad). The following gene-specific primer pairs were used: *Dmrt2.1*-Forward and *Dmrt2.2/2.3*-Forward 5'-*AGGGGCTTTCTGGGAAACAG*-3', *Dmrt2.1*-Reverse 5'-*CGTCATTGGGCGATAACCTTC*-3', *Dmrt2.2/2.3*-Reverse 5'-*TAGAATAATCCAAGGAGAACTTC*-3', *GFP*-Forward 5'-*CAACCACTACCTGAGCACCC*-3', *GFP*-Reverse 5'-*GTCCATGCCGAGAGTGATCC*-3', *Gus*-Forward 5'-*AGCCGCTACGGGAGTCG*-3' and *Gus*-Reverse 5'-GCTGCTTCTTGGGTGATGTCA-3'. *Dmrt2* and *GFP* expression levels were quantified in triplicates and normalized to *Gus* expression levels. Resultant data were analyzed using the comparative Ct method.

***In utero* electroporation (IUE) and plasmids**

IUE was performed as previously described in Briz *et al.* [63]. Briefly, the mixture composed of: a plasmid expressing GFP or DsRed fluorescent protein (1 µg/µl), 0.1% Fast Green FCF (F7252, Sigma) and, in the case of silencing or overexpression experiments, sh*Dmrt2* or *pCAG-Dmrt2.1* plasmid (1 µg/µl) respectively, was injected into the left lateral ventricle of E13.5 embryos using pulled glass micropipettes. Five voltage pulses (40 mv, 50 ms) were applied using external paddles oriented to target the cingulate cortex. By E15.5 and E18.5, GFP- or Red-brain embryos were selected for further analyses.

Plasmids used were *pCAG-GFP* (#11150, Addgene); *pCAGGs-DsRedExpress* (gift from Marta Nieto); *Dmrt2* short hairpins, sh*Dmrt2*_1 and sh*Dmrt2*_2, in pLKO.1 vector were acquired in Sigma-Aldrich [hairpin sequences are sh*Dmrt2*_1:

AGCAGACGCTCAGCGACAAAT (TRCN0000418486) and, sh*Dmrt2*_2: *GCCACAACTTACAGACAATAT* (TRCN0000086379)] (see **Figure 1E** for approximate location of each sh in the *Dmrt2* locus).

Dmrt2.1 cDNA was cloned into the pCAG backbone obtained from the double-digested *pCAG-GFP* plasmid (#11150, Addgene) by EcoRI (10703737001, Roche) and NotI (11037668001, Roche). cDNA was isolated from the *Dmrt2*-probe plasmid, kindly provided by Takahiko Sato[16]. The primers used were: Forward 5'-*TATCGAATTCTGGCCACCATGACGGAAGGGCAGGCAG*-3', including EcoRI-recognition and Kozak sequences, and Reverse 5'-*GATTGCGGCCGCTTTACTGAGAGACGTGAGTGAC*-3', including NotI-recognition sequence. The ligation reaction was carried out using the DNA ligase T4 (M0202L, New England BioLabs) in T4 ligase buffer (B0202S, New England Biolabs) according to the manufacturer's specifications.

RNA-Sequencing and FACSorting

For the RNA-Seq, embryos were electroporated with pCGA-DSRed Express and sh*Dmrt2* as previously described. At E18.5, individual embryos with fluorescence signal were selected, and brains were collected on ice-cold D-PBS (14287-072, Gibco™). After meninges' removal, cingulate cortices were isolated, finely chopped and digested for 15 min in D-PBS containing Liberase 0.15 mg/ml (05 401 119 001, Roche), 300 U of DNase I (18047019, Invitrogen™). After addition of D-PBS-/0.05% Fetal Bovine Serum (FBS) (A5256701, Gibco), the tissue was mechanically dissociated with 230 mm-length glass Pasteur pipettes (702, Deltalab), whose tips have been previously fire-polished reduced five times. Cell debris was eliminated using Debris Removal Solution (130-109-398, Miltenyi Biotec) following the manufacturer's specifications and the pellet was recovered. Cells were resuspended in sorting medium [0,5% FBS, trehalose 0.05 mg/ml (T9531, Sigma) and in D-PBS]. Samples were not pooled and each sample corresponded to one single DsRed(+)mouse brain. Lastly, cells were sorted using FACSAria™ Fusion Cell Sorter (BD Biosciences). Cell fluorescence size, complexity and intensity were acquired with BD FACSDiva™ 8.0 Software. Analysis was performed using FlowJo™ v10.9 Software (BD Life Sciences).

Sorted cell suspension was treated with 100 U of DNase I (18047019, Invitrogen™), RNA was extracted and purified with RNeasy® Plus Micro Kit (74034, Qiagen) following the manufacturer's protocol. RNA quality was assessed with Agilent 2100 Bioanalyzer System. Only samples with RNA integrity number (RIN) values between 9.9 and 10 were processed for sequencing. For the RNA-Seq ultra-low input poly-A selection, each sample was processed to generate a dataset (minimum of 8 M reads per sample) at a

50 nt read length in single-end format (1x50) and sequenced in NextSeq 2000 system (Illumina) at the Center for Genomic Regulation (CRG) Core Facility.

Sequence quality was determined with FastQC v0.11.8 software [64], revealing over 32 million mean reads with median and mean base quality over 32 using Phred+33 quality score. Two reference genome versions were created based on Ensembl *Mus musculus* (GRCm39; https://www.ncbi.nlm.nih.gov/assembly/GCF_000001635.27): the Y chromosome hard masked (Y-masked) and the Y chromosome with PARs hard masked (YPARs-masked) based on Olney *et al.* [65]. Reads were aligned with Hisat2 v2.1.0 [66] to the masked versions of the reference genome. Aligned reads were further processed using Samtools v1.21 [67] and quantified to gene level using htseq-count v0.11.2 [68] and GTF annotation file. Whole-genome alignments were visualized with Integrative Genomics Viewer (IGV) [69]. RNA-seq data sets can be accessed at the European Nucleotide Archive (ENA) public repository under the following accession numbers (PRJEB56430/ERA18509105).

Differential expression analysis was performed using the Bioconductor package Deseq2 v1.14.0 [70]. Differential expressed genes (DEGs) data were processed with custom R scripts (R v4.4) considering genes with q-value < 0.05 and |log2 fold change| > 1 as significantly up- or downregulated. Gene Set Enrichment Analysis (GSEA)[71] was performed using R packages clusterProfiler[72] and enrichplot (DOI: 10.18129/B9.bioc.enrichplot) for the statistical analysis and visualization of functional profiles of genes and gene clusters. All graphs were plotted with ggplot2 and GOplot R package [73].

Statistical Analyses

The researchers were blinded to the sex and genotype at the time of analysis. The number of quantified animals is indicated in each plot; a minimum of three mice were included. The normality of the distribution was tested using the Shapiro-Wilk test in all cases. Each individual test is indicated in the figure legend of the corresponding experiments. Statistically significant differences were considered and represented by p-value: *p < 0.05 and **p < 0.01. All statistical analyses were determined using GraphPad Prism 9.

ACKNOWLEDGMENTS

We thank Takahiko Sato for providing the *Dmrt2* probe and Marta Nieto for the *pCAG-GFP* and *pCAGGs-DsRedExpress* plasmids. The Advanced Light Microscopy, Flow Cytometry, Animal facilities, and the Genomics and NGS Core Facility (GENGS) at the CBM (CSIC-UAM) performed next-generation sequencing data analysis. We also thank

Paola Bovolenta, Marta Nieto, Jorge García Marqués, and Leo Beccari for critical reading and advice.
Grant PGC2018-101751-A-100 and PID2021-127235NB-I00 funded by MCIN/AEI/ 10.13039/501100011033, and ERDF, “A way of making Europe”.
AB-S. holds an FPI fellowship from the Spanish MCIN, PRE19-089366. RTC holds an FPI from the CAM, PIPF-2022/SAL-GL-24909, cofounded by ESF. ES-S. was supported by Grant RYC-2016-20537 funded by MCIN/AEI/10.13039/501100011033 and ESF, “Investing in your future”.
During the preparation of this work, the authors used “*perplexity.ai”* to edit the text. After using this tool, the authors reviewed and edited the content as needed and take full responsibility for the publication's content.

FIGURE LEGENDS

Figure 1. *Dmrt2* is expressed in the deep-layer neurons of the cingulate cortex at higher levels in male mice during early cortical development. In all panels, *Dmrt2* was detected by ISH **A)** *Dmrt2* in the mantle zone of male and female embryos at E14.5. (a’, a’’). Insets show a higher magnification of the cingulate primordium. **B)** By E18.5, ***Dmrt2* occupies the entire cingulate cortex in its rostrocaudal axis**. Only male images are depicted. Each coronal section in b’-b’’’ corresponds to the sagittal level indicated with a dashed line in the left panel. **C-D) *Dmrt2* expression in postnatal cingulate cortices at P7**. In the anterior cingulate cortex, *Dmrt2* overlaps with TBR1 (c’, d’) and SATB2 in more superficial layers (c’’). Additionally, in the mid-cingulate, *Dmrt2* colocalizes with CTIP2 (d’’). cc: corpus callosum. Scale bar: 250 µm, except in the indicated cases. **E) *Dmrt2* locus schematic.** Solid black and grey boxes represent exons; white boxes represent untranslated regions (UTR); the green box within exon 2 indicates the location of the DM domain; purple line, *Dmrt2* riboprobe used for ISH detection; blue and pink line, interference RNAs used in this study to target *Dmrt2*. **F) *Dmrt2.1* transcriptional variant is higher in males in early development.** RT-qPCR analyzed cingulate cortices of male and female embryos with the primers depicted in E) (red arrows) at several time points throughout development. The graph represents mean±SEM in arbitrary units (au). Each dot corresponds to one individual embryo. Two-tailed t-test: * p-value < 0.05 ($n \geq 5$).

Supplementary Figure 1 (related to **Figure 1**). ***Dmrt2* is expressed in deeper-layer neurons of the mouse cingulate cortex throughout development. A) *Dmrt2* ISH in female embryos at E18.5 shows a similar pattern to male embryos**. (a’, a’’) Coronal sections corresponding to the rostrocaudal positions are depicted in the sagittal view (left

panel). **B) *Dmrt2* is maintained in male and female adult animals** along the anteroposterior axis, showing in coronal views. A: anterior, P: posterior. **C-D) *Dmrt2* co-staining with TBR1 and SABT2 at E18.5 (C) and P7 (D).** (c'-c'', d') Insets of deep layers of the cingulate cortex. Scale bar: 250 µm, except in the indicated cases. (*) indicates broken tissue.

Supplementary Figure 2 (related to **Figure 1**). ***Dmrt2* transcriptional variants display a dynamic expression during development. A) *Dmrt2* locus and the three putative transcriptional variants** according to NCBI genome browser (Gene ID: 226049)**.** Solid black and grey boxes represent exons; white boxes represent untranslated regions (UTR); green box within exon 2, the DM domain; purple line, *Dmrt2* riboprobe used for ISH detection; red and orange arrows represent qPCR primers; blue and pink lines represent interference RNAs used in this study to target *Dmrt2.* **B) *Dmrt2.2/2.3* relative expression analyzed across development.** Contrary to *Dmrt2.1* variant (**Figure 1**), no differences were observed between the sexes for *Dmrt2.2/2.3*. Cingulate cortices of males and females were analyzed by qPCR at the indicated time points. Results are the mean±SEM. Each dot corresponds to one individual embryo. Two-tailed t-test: not significant (n.s) p-value > 0.05 ($n \geq 5$).

Figure 2. *Dmrt2* downregulation alters the development of cingulate cortical neurons. A-D) Representative images of E18.5-electroporated brains at E13.5. **A) Male mock, B) Male sh*Dmrt2*, C) Female mock, and D) Female sh*Dmrt2*.** The electroporated (red dashed circled) area is quantified in E). **a'-d')** Higher magnification of the cingulate cortex in the four conditions. The red box area was divided into 10 bins to cover the cortical plate of the CgCx and fluorescence was quantified in F). White arrowheads indicate ectopic GFP(+) cells in the cc of sh*Dmrt2*-treated animals, quantified in G. **a''-d''**) Higher magnification for the ventricular zone (VZ). In *shDmrt2* animals, GFP(+) cells are not visible in this area. The white line delimits the lateral ventricle (LV). **a'''-d'''**). Higher magnification of the GFP(+) projections towards the thalamus across the cc, above the internal capsule. White arrows indicate lateral misguidance. **E) Decrease in the total GFP fluorescence intensity in male embryos**. The IUE area was quantified by measuring the GFP fluorescence, which was determined by integrated density (IntDen). Two-tailed t-test (n = 5). **F) Cellular distribution of GFP(+) cells in the medial CgCx.** The histogram represents each bin's GFP fluorescence intensity (IntDen), marked in a'-d'. Solid bars depict mock embryos, while empty bars represent *shDmrt2*-treated animals. Two-tailed t-test ($n \geq 5$). **G) Count of the GFP(+) staked cells in sh*Dmrt2* brains.** Two-tailed t-test (n = 5). In scatter plots,

each dot represents individual embryos. In all graphs, the results correspond to the mean±SEM of the average of three sections per embryo, and the significance is as follows: * p-value < 0.05 and ** p-value < 0.01.

Supplementary Figure 3 (related to **Figure 2**). ***Dmrt2* silencing causes phenotypic alterations in the CgCx. A) Summary of experimental design.** In this study, all brains were electroporated at E13.5 and then analyzed either at E15.5 or E18.5, depending on the experiment. **Right panel, GFP region in an E15.5 electroporated brain. B) *Dmrt2* is downregulated after sh*Dmrt2* IUE.** qRT-PCR analysis of sh*Dmrt2* effect on *Dmrt2* expression in E18.5 electroporated brains. The graph depicts the *Dmrt2* expression ratio between the ipsilateral versus the contralateral hemisphere of each animal. Colored dots (green for males, purple for females) represent the animals with reduced *Dmrt2* levels. **C-F) Representative sequential sections across the rostrocaudal axis from E18.5 brains, electroporated at E13.5. C) Male mock, D) Male sh*Dmrt2*, E) Female mock, and F) Female sh*Dmrt2*.** Insets in D and F correspond to panels in G**.** (A: anterior and P: posterior). **G) GFP(+) cells stacked at the corpus callosum**. All colocalize with TBR1 and CTIP2, but only a few with SATB2. White arrowheads correspond to GFP and SATB2 colocalization. **H) Cellular distribution of GFP(+) cells in the medial CgCx.** Two-tailed t-test (n = 5). Each dot represents an individual embryo. The graph shows the mean±SEM of the average of three sections per embryo, and the significance is as follows: *p-value < 0.05 and **p-value < 0.01.

Figure 3. *Dmrt2* downregulation affects the proliferation of CgCx progenitors more strongly in male embryos. A-D) E15.5 CgCx primordium of electroporated embryos at E13.5. GFP(+) cells populate the three layers VZ/SVZ, IZ and CP (TBR1+). **A) Male mock, B) Male sh*Dmrt2*, C) Female mock, D) Female sh*Dmrt2***. White arrowheads in B and D point to the somas of the few GFP(+) cells that reached the CP and indicate a stronger effect in males quantified in E-G. **E) Total GFP cellular density within the three layers.** Tukey's multiple comparison test, ordinary one-way ANOVA (n ≥ 5). **F) Quantifications of GFP(+) cellular distribution**. Dunn's multiple comparison test, Kruskal-Wallis test (n ≥ 5). **G) Cellular density in each layer in the four conditions.** Tukey's multiple comparison test, ordinary one-way ANOVA (n = 6). For all graphs, each dot corresponds to one individual embryo; results are expressed as mean ± SEM, and significances are as follows: * p-value < 0.05 and ** p-value < 0.01.

Supplementary Figure 4 (related to **Figure 3**). **A) GFP(+) distribution in cingulate primordium layers at E15.5 in female mock**. **B) At E15.5, *Dmrt2*, detected by FISH,**

is located in the CP. **C)** GFP distribution in an E15.5 embryo electroporated at E13.5 with a different sh*Dmrt2* (sh*Dmrt2*_2; see Figure 1E for approximate location in *Dmrt2* locus). Similar phenotypes between the two sh*Dmrt2* iRNA are observed. **D-G) *Dmrt2.1* overexpression (oe) produces the opposite effect of *Dmrt2* downregulation. D)** E15.5 CgCx primordium of electroporated embryos at E13.5. **E-G)** Quantification of *Dmrt2.1* phenotype: **E) Total GFP cellular density within the three layers.** Tukey's multiple comparison test, ordinary one-way ANOVA (n ≥ 4). **F) Cellular density in each layer in the four conditions.** Dunn's multiple comparison test, Kruskal-Wallis test (n ≥ 4) **G) Quantifications of GFP(+) cellular distribution.** Tukey's multiple comparison test, ordinary one-way ANOVA (≥ 4). For all graphs, each dot corresponds to one individual embryo; results are expressed as mean ± SEM and significance mean * p-value < 0.05. **H) Quantification values** (mean ± SEM) cellular distribution percentages and cellular densities in mock, sh*Dmrt2*_1, and oe*Dmrt2.1* conditions.

Figure 4. *Dmrt2* controls neuronal differentiation in post-mitotic neurons. A) Two-dimensional PCA plot for the four experimental conditions shows the clustering of mock separated from sh*Dmrt2* samples. Among the sh*Dmrt2* group, male and female samples show less clear clustering than in mock conditions. **B)** Volcano plots represent DEGs in sh*Dmrt2* vs. mock comparisons (**Supplementary Tables 3 and 4**). Blue indicates downregulated genes, and red indicates upregulated genes (numbers in brackets). More DEGs are retrieved in female comparisons (1163) than male ones (488). The trend in down- and up-regulated DEGs is similar in the two sexes. The Venn Diagram indicates the number of DEGs shared (306) by male and female comparisons. **C-F) Female sh*Dmrt2* vs. mock DEGs analysis. C)** GSEA on down-regulated DEGs shows neuron-related overrepresented categories. 15 categories with NES < -2 (out of 136; **Supplementary Table 3**) are shown in the bar plot. **D)** Among the 15 down-regulated categories, genes with changes between log2 FC of -2.13 and -1.51 are represented in the GO-Chord plot. **E)** GSEA on up-regulated DEGs are related to immune system and cell cycle. 15 categories with a NES score > 2 (out of 159, **Supplementary Table 3**) are shown in the bar plot. **F)** Among the 15 up-regulated categories, genes with changes between log2 FC of 1.5 and 3.5 are represented in the GO-Chord plot.

Supplementary Figure 5 (related to **Figure 4**). **A)** Heatmaps of DEGs for all comparisons. The color and intensity in the heatmap represent changes in gene expression from the list of genes with |log2FC|<0.5 p-adj < 0.05. **B)** Volcano plots represent DEGs in male vs. female comparisons. Blue color indicates downregulated genes, and red indicates upregulated genes (numbers in brackets). **C)** *Dmrt2*

downregulation in RNA-seq samples. Number of *Dmrt2* reads in the four groups. Two-tailed t-test: * p-value < 0.05 (n ≥ 4). **D-E) Male-specific sh*Dmrt2* vs. mock DEGs analysis. D)** GSEA for down- and up-regulated DEGs (182 DEGs in the Venn Diagram in **Figure 4**). All categories with a NES > |1.9| are shown. **E)** Among the categories depicted in D), genes with a log2 FC between -3 and 3 are shown in a GO-Chord plot.

REFERENCES

1. Zagni, E., Simoni, L., and Colombo, D. (2016). Sex and Gender Differences in Central Nervous System-Related Disorders. Neurosci J *2016*, 2827090. 10.1155/2016/2827090.
2. McCarthy, M.M., Pickett, L.A., VanRyzin, J.W., and Kight, K.E. (2015). Surprising origins of sex differences in the brain. Horm Behav *76*, 3-10. 10.1016/j.yhbeh.2015.04.013.
3. Casado-Navarro, R., and Serrano-Saiz, E. (2022). DMRT Transcription Factors in the Control of Nervous System Sexual Differentiation. Front Neuroanat *16*, 937596. 10.3389/fnana.2022.937596.
4. Kopp, A. (2012). Dmrt genes in the development and evolution of sexual dimorphism. Trends Genet *28*, 175-184. 10.1016/j.tig.2012.02.002.
5. Zarkower, D., and Murphy, M.W. (2022). DMRT1: An Ancient Sexual Regulator Required for Human Gonadogenesis. Sex Dev *16*, 112-125. 10.1159/000518272.
6. Murphy, M.W., Lee, J.K., Rojo, S., Gearhart, M.D., Kurahashi, K., Banerjee, S., Loeuille, G.A., Bashamboo, A., McElreavey, K., Zarkower, D., et al. (2015). An ancient protein-DNA interaction underlying metazoan sex determination. Nat Struct Mol Biol *22*, 442-451. 10.1038/nsmb.3032.
7. Goodwin, S.F., and Hobert, O. (2021). Molecular Mechanisms of Sexually Dimorphic Nervous System Patterning in Flies and Worms. Annu Rev Cell Dev Biol *37*, 519-547. 10.1146/annurev-cellbio-120319-115237.
8. Serrano-Saiz, E., and Isogai, Y. (2021). Single-cell molecular and developmental perspectives of sexually dimorphic circuits underlying innate social behaviors. Curr Opin Neurobiol *68*, 159-166. 10.1016/j.conb.2021.03.010.
9. Kikkawa, T., and Osumi, N. (2021). Multiple Functions of the Dmrt Genes in the Development of the Central Nervous System. Front Neurosci *15*, 789583. 10.3389/fnins.2021.789583.
10. Young, F.I., Keruzore, M., Nan, X., Gennet, N., Bellefroid, E.J., and Li, M. (2017). The doublesex-related Dmrta2 safeguards neural progenitor maintenance involving transcriptional regulation of Hes1. Proc Natl Acad Sci U S A *114*, E5599-E5607. 10.1073/pnas.1705186114.
11. Konno, D., Kishida, C., Maehara, K., Ohkawa, Y., Kiyonari, H., Okada, S., and Matsuzaki, F. (2019). Dmrt factors determine the positional information of cerebral cortical progenitors via differential suppression of homeobox genes. Development *146*. 10.1242/dev.174243.
12. Yoshizawa, A., Nakahara, Y., Izawa, T., Ishitani, T., Tsutsumi, M., Kuroiwa, A., Itoh, M., and Kikuchi, Y. (2011). Zebrafish Dmrta2 regulates neurogenesis in the telencephalon. Genes Cells *16*, 1097-1109. 10.1111/j.1365-2443.2011.01555.x.
13. Bellefroid, E.J., Leclere, L., Saulnier, A., Keruzore, M., Sirakov, M., Vervoort, M., and De Clercq, S. (2013). Expanding roles for the evolutionarily conserved Dmrt sex transcriptional regulators during embryogenesis. Cellular and molecular life sciences : CMLS *70*, 3829-3845. 10.1007/s00018-013-1288-2.

14. Kikkawa, T., Obayashi, T., Takahashi, M., Fukuzaki-Dohi, U., Numayama-Tsuruta, K., and Osumi, N. (2013). Dmrta1 regulates proneural gene expression downstream of Pax6 in the mammalian telencephalon. Genes Cells *18*, 636-649. 10.1111/gtc.12061.
15. Galazo, M.J., Emsley, J.G., and Macklis, J.D. (2016). Corticothalamic Projection Neuron Development beyond Subtype Specification: Fog2 and Intersectional Controls Regulate Intraclass Neuronal Diversity. Neuron *91*, 90-106. 10.1016/j.neuron.2016.05.024.
16. Seo, K.W., Wang, Y., Kokubo, H., Kettlewell, J.R., Zarkower, D.A., and Johnson, R.L. (2006). Targeted disruption of the DM domain containing transcription factor Dmrt2 reveals an essential role in somite patterning. Dev Biol *290*, 200-210. 10.1016/j.ydbio.2005.11.027.
17. Sato, T., Rocancourt, D., Marques, L., Thorsteinsdottir, S., and Buckingham, M. (2010). A Pax3/Dmrt2/Myf5 regulatory cascade functions at the onset of myogenesis. PLoS Genet *6*, e1000897. 10.1371/journal.pgen.1000897.
18. Ono, K., Hata, K., Nakamura, E., Ishihara, S., Kobayashi, S., Nakanishi, M., Yoshida, M., Takahata, Y., Murakami, T., Takenoshita, S., et al. (2021). Dmrt2 promotes transition of endochondral bone formation by linking Sox9 and Runx2. Commun Biol *4*, 326. 10.1038/s42003-021-01848-1.
19. Gunes, S., Ekinci, O., Ekinci, N., and Toros, F. (2017). Coexistence of 9p Deletion Syndrome and Autism Spectrum Disorder. J Autism Dev Disord *47*, 520-521. 10.1007/s10803-016-2943-x.
20. Vinci, G., Chantot-Bastaraud, S., El Houate, B., Lortat-Jacob, S., Brauner, R., and McElreavey, K. (2007). Association of deletion 9p, 46,XY gonadal dysgenesis and autistic spectrum disorder. Mol Hum Reprod *13*, 685-689. 10.1093/molehr/gam045.
21. Hanna, G.L., Veenstra-VanderWeele, J., Cox, N.J., Boehnke, M., Himle, J.A., Curtis, G.C., Leventhal, B.L., and Cook, E.H., Jr. (2002). Genome-wide linkage analysis of families with obsessive-compulsive disorder ascertained through pediatric probands. Am J Med Genet *114*, 541-552. 10.1002/ajmg.10519.
22. Willour, V.L., Yao Shugart, Y., Samuels, J., Grados, M., Cullen, B., Bienvenu, O.J., 3rd, Wang, Y., Liang, K.Y., Valle, D., Hoehn-Saric, R., et al. (2004). Replication study supports evidence for linkage to 9p24 in obsessive-compulsive disorder. Am J Hum Genet *75*, 508-513. 10.1086/423899.
23. Deng, M., Wang, Y., Yu, S., Fan, Q., Qiu, J., Wang, Z., and Xiao, Z. (2022). Exploring Association Between Serotonin and Neurogenesis Related Genes in Obsessive-Compulsive Disorder in Chinese Han People: Promising Association Between DMRT2, miR-30a-5p, and Early-Onset Patients. Front Psychiatry *13*, 857574. 10.3389/fpsyt.2022.857574.
24. Zhang, X., Zhang, J., Liu, Q., Zhao, Y., Zhang, W., and Yang, H. (2020). Circ-CUX1 Accelerates the Progression of Neuroblastoma via miR-16-5p/DMRT2 Axis. Neurochem Res *45*, 2840-2855. 10.1007/s11064-020-03132-w.
25. Bedogni, F., Hodge, R.D., Elsen, G.E., Nelson, B.R., Daza, R.A., Beyer, R.P., Bammler, T.K., Rubenstein, J.L., and Hevner, R.F. (2010). Tbr1 regulates regional and laminar identity of postmitotic neurons in developing neocortex. Proc Natl Acad Sci U S A *107*, 13129-13134. 10.1073/pnas.1002285107.
26. McKenna, W.L., Betancourt, J., Larkin, K.A., Abrams, B., Guo, C., Rubenstein, J.L., and Chen, B. (2011). Tbr1 and Fezf2 regulate alternate corticofugal neuronal identities during neocortical development. J Neurosci *31*, 549-564. 10.1523/JNEUROSCI.4131-10.2011.

27. Alcamo, E.A., Chirivella, L., Dautzenberg, M., Dobreva, G., Farinas, I., Grosschedl, R., and McConnell, S.K. (2008). Satb2 regulates callosal projection neuron identity in the developing cerebral cortex. Neuron *57*, 364-377. 10.1016/j.neuron.2007.12.012.
28. Woodworth, M.B., Greig, L.C., Kriegstein, A.R., and Macklis, J.D. (2012). SnapShot: cortical development. Cell *151*, 918-918 e911. 10.1016/j.cell.2012.10.004.
29. Hevner, R.F. (2019). Intermediate progenitors and Tbr2 in cortical development. J Anat *235*, 616-625. 10.1111/joa.12939.
30. Neumann, H., Schweigreiter, R., Yamashita, T., Rosenkranz, K., Wekerle, H., and Barde, Y.A. (2002). Tumor necrosis factor inhibits neurite outgrowth and branching of hippocampal neurons by a rho-dependent mechanism. J Neurosci *22*, 854-862. 10.1523/JNEUROSCI.22-03-00854.2002.
31. Soleman, S., Filippov, M.A., Dityatev, A., and Fawcett, J.W. (2013). Targeting the neural extracellular matrix in neurological disorders. Neuroscience *253*, 194-213. 10.1016/j.neuroscience.2013.08.050.
32. Hirano, S., and Takeichi, M. (2012). Cadherins in brain morphogenesis and wiring. Physiol Rev *92*, 597-634. 10.1152/physrev.00014.2011.
33. Martinez-Garay, I. (2020). Molecular Mechanisms of Cadherin Function During Cortical Migration. Front Cell Dev Biol *8*, 588152. 10.3389/fcell.2020.588152.
34. Bandtlow, C.E., and Zimmermann, D.R. (2000). Proteoglycans in the developing brain: new conceptual insights for old proteins. Physiol Rev *80*, 1267-1290. 10.1152/physrev.2000.80.4.1267.
35. Faissner, A., Pyka, M., Geissler, M., Sobik, T., Frischknecht, R., Gundelfinger, E.D., and Seidenbecher, C. (2010). Contributions of astrocytes to synapse formation and maturation - Potential functions of the perisynaptic extracellular matrix. Brain Res Rev *63*, 26-38. 10.1016/j.brainresrev.2010.01.001.
36. Ottolenghi, C., Veitia, R., Barbieri, M., Fellous, M., and McElreavey, K. (2000). The human doublesex-related gene, DMRT2, is homologous to a gene involved in somitogenesis and encodes a potential bicistronic transcript. Genomics *64*, 179-186. 10.1006/geno.2000.6120.
37. Pointis, G., Latreille, M.T., Mignot, T.M., Janssens, Y., and Cedard, L. (1979). Regulation of testosterone synthesis in the fetal mouse testis. J Steroid Biochem *11*, 1609-1612. 10.1016/0022-4731(79)90357-1.
38. Clough, E., Jimenez, E., Kim, Y.A., Whitworth, C., Neville, M.C., Hempel, L.U., Pavlou, H.J., Chen, Z.X., Sturgill, D., Dale, R.K., et al. (2014). Sex- and tissue-specific functions of Drosophila doublesex transcription factor target genes. Developmental cell *31*, 761-773. 10.1016/j.devcel.2014.11.021.
39. Woodworth, M.B., Greig, L.C., Liu, K.X., Ippolito, G.C., Tucker, H.O., and Macklis, J.D. (2016). Ctip1 Regulates the Balance between Specification of Distinct Projection Neuron Subtypes in Deep Cortical Layers. Cell Rep *15*, 999-1012. 10.1016/j.celrep.2016.03.064.
40. Leone, D.P., Heavner, W.E., Ferenczi, E.A., Dobreva, G., Huguenard, J.R., Grosschedl, R., and McConnell, S.K. (2015). Satb2 Regulates the Differentiation of Both Callosal and Subcerebral Projection Neurons in the Developing Cerebral Cortex. Cereb Cortex *25*, 3406-3419. 10.1093/cercor/bhu156.
41. Ji, J.F., He, B.P., Dheen, S.T., and Tay, S.S. (2004). Expression of chemokine receptors CXCR4, CCR2, CCR5 and CX3CR1 in neural progenitor cells isolated from the subventricular zone of the adult rat brain. Neurosci Lett *355*, 236-240. 10.1016/j.neulet.2003.11.024.

42. Wiegreffe, C., Simon, R., Peschkes, K., Kling, C., Strehle, M., Cheng, J., Srivatsa, S., Liu, P., Jenkins, N.A., Copeland, N.G., et al. (2015). Bcl11a (Ctip1) Controls Migration of Cortical Projection Neurons through Regulation of Sema3c. Neuron *87*, 311-325. 10.1016/j.neuron.2015.06.023.
43. Hippenmeyer, S. (2014). Molecular pathways controlling the sequential steps of cortical projection neuron migration. Adv Exp Med Biol *800*, 1-24. 10.1007/978-94-007-7687-6_1.
44. de Haas, A.H., van Weering, H.R., de Jong, E.K., Boddeke, H.W., and Biber, K.P. (2007). Neuronal chemokines: versatile messengers in central nervous system cell interaction. Mol Neurobiol *36*, 137-151. 10.1007/s12035-007-0036-8.
45. Li, M., and Ransohoff, R.M. (2008). Multiple roles of chemokine CXCL12 in the central nervous system: a migration from immunology to neurobiology. Prog Neurobiol *84*, 116-131. 10.1016/j.pneurobio.2007.11.003.
46. Watson, A.E.S., Goodkey, K., Footz, T., and Voronova, A. (2020). Regulation of CNS precursor function by neuronal chemokines. Neurosci Lett *715*, 134533. 10.1016/j.neulet.2019.134533.
47. Rubin, J.D., Stanley, J.T., Sigauke, R.F., Levandowski, C.B., Maas, Z.L., Westfall, J., Taatjes, D.J., and Dowell, R.D. (2021). Transcription factor enrichment analysis (TFEA) quantifies the activity of multiple transcription factors from a single experiment. Commun Biol *4*, 661. 10.1038/s42003-021-02153-7.
48. Naqvi, S., Kim, S., Hoskens, H., Matthews, H.S., Spritz, R.A., Klein, O.D., Hallgrimsson, B., Swigut, T., Claes, P., Pritchard, J.K., and Wysocka, J. (2023). Precise modulation of transcription factor levels identifies features underlying dosage sensitivity. Nat Genet *55*, 841-851. 10.1038/s41588-023-01366-2.
49. Kimura, K., Hachiya, T., Koganezawa, M., Tazawa, T., and Yamamoto, D. (2008). Fruitless and doublesex coordinate to generate male-specific neurons that can initiate courtship. Neuron *59*, 759-769. 10.1016/j.neuron.2008.06.007.
50. Rideout, E.J., Dornan, A.J., Neville, M.C., Eadie, S., and Goodwin, S.F. (2010). Control of sexual differentiation and behavior by the doublesex gene in Drosophila melanogaster. Nat Neurosci *13*, 458-466. 10.1038/nn.2515.
51. Sanders, L.E., and Arbeitman, M.N. (2008). Doublesex establishes sexual dimorphism in the Drosophila central nervous system in an isoform-dependent manner by directing cell number. Dev Biol *320*, 378-390. 10.1016/j.ydbio.2008.05.543.
52. Yang, W., Warrington, N.M., Taylor, S.J., Whitmire, P., Carrasco, E., Singleton, K.W., Wu, N., Lathia, J.D., Berens, M.E., Kim, A.H., et al. (2019). Sex differences in GBM revealed by analysis of patient imaging, transcriptome, and survival data. Sci Transl Med *11*. 10.1126/scitranslmed.aao5253.
53. Apps, M.A., Rushworth, M.F., and Chang, S.W. (2016). The Anterior Cingulate Gyrus and Social Cognition: Tracking the Motivation of Others. Neuron *90*, 692-707. 10.1016/j.neuron.2016.04.018.
54. Stevens, J.S., and Hamann, S. (2012). Sex differences in brain activation to emotional stimuli: a meta-analysis of neuroimaging studies. Neuropsychologia *50*, 1578-1593. 10.1016/j.neuropsychologia.2012.03.011.
55. Pujol, J., Lopez, A., Deus, J., Cardoner, N., Vallejo, J., Capdevila, A., and Paus, T. (2002). Anatomical variability of the anterior cingulate gyrus and basic dimensions of human personality. Neuroimage *15*, 847-855. 10.1006/nimg.2001.1004.

56. Francis-Oliveira, J., Leitzel, O., and Niwa, M. (2022). Are the Anterior and Mid-Cingulate Cortices Distinct in Rodents? Front Neuroanat *16*, 914359. 10.3389/fnana.2022.914359.
57. Liu, R.H., Xue, M., Li, X.H., and Zhuo, M. (2020). Sex difference in synaptic plasticity in the anterior cingulate cortex of adult mice. Mol Brain *13*, 41. 10.1186/s13041-020-00583-8.
58. Ounap, K., Uibo, O., Zordania, R., Kiho, L., Ilus, T., Oiglane-Shlik, E., and Bartsch, O. (2004). Three patients with 9p deletions including DMRT1 and DMRT2: a girl with XY complement, bilateral ovotestes, and extreme growth retardation, and two XX females with normal pubertal development. Am J Med Genet A *130A*, 415-423. 10.1002/ajmg.a.30269.
59. Hernandez-Miranda, L.R., Muller, T., and Birchmeier, C. (2017). The dorsal spinal cord and hindbrain: From developmental mechanisms to functional circuits. Dev Biol *432*, 34-42. 10.1016/j.ydbio.2016.10.008.
60. Andersson, L.S., Larhammar, M., Memic, F., Wootz, H., Schwochow, D., Rubin, C.J., Patra, K., Arnason, T., Wellbring, L., Hjalm, G., et al. (2012). Mutations in DMRT3 affect locomotion in horses and spinal circuit function in mice. Nature *488*, 642-646. 10.1038/nature11399.
61. McFarlane, L., Truong, V., Palmer, J.S., and Wilhelm, D. (2013). Novel PCR assay for determining the genetic sex of mice. Sex Dev *7*, 207-211. 10.1159/000348677.
62. Di Meglio, T., Kratochwil, C.F., Vilain, N., Loche, A., Vitobello, A., Yonehara, K., Hrycaj, S.M., Roska, B., Peters, A.H., Eichmann, A., et al. (2013). Ezh2 orchestrates topographic migration and connectivity of mouse precerebellar neurons. Science *339*, 204-207. 10.1126/science.1229326.
63. Briz, C.G., Navarrete, M., Esteban, J.A., and Nieto, M. (2017). In Utero Electroporation Approaches to Study the Excitability of Neuronal Subpopulations and Single-cell Connectivity. J Vis Exp. 10.3791/55139.
64. Wingett, S.W., and Andrews, S. (2018). FastQ Screen: A tool for multi-genome mapping and quality control. F1000Res *7*, 1338. 10.12688/f1000research.15931.2.
65. Olney, K.C., Brotman, S.M., Andrews, J.P., Valverde-Vesling, V.A., and Wilson, M.A. (2020). Reference genome and transcriptome informed by the sex chromosome complement of the sample increase ability to detect sex differences in gene expression from RNA-Seq data. Biol Sex Differ *11*, 42. 10.1186/s13293-020-00312-9.
66. Kim, D., Langmead, B., and Salzberg, S.L. (2015). HISAT: a fast spliced aligner with low memory requirements. Nature methods *12*, 357-360. 10.1038/nmeth.3317.
67. Li, H., Handsaker, B., Wysoker, A., Fennell, T., Ruan, J., Homer, N., Marth, G., Abecasis, G., Durbin, R., and Genome Project Data Processing, S. (2009). The Sequence Alignment/Map format and SAMtools. Bioinformatics *25*, 2078-2079. 10.1093/bioinformatics/btp352.
68. Anders, S., Pyl, P.T., and Huber, W. (2015). HTSeq--a Python framework to work with high-throughput sequencing data. Bioinformatics *31*, 166-169. 10.1093/bioinformatics/btu638.
69. Thorvaldsdottir, H., Robinson, J.T., and Mesirov, J.P. (2013). Integrative Genomics Viewer (IGV): high-performance genomics data visualization and exploration. Brief Bioinform *14*, 178-192. 10.1093/bib/bbs017.

70. Love, M.I., Huber, W., and Anders, S. (2014). Moderated estimation of fold change and dispersion for RNA-seq data with DESeq2. Genome Biol *15*, 550. 10.1186/s13059-014-0550-8.
71. Subramanian, A., Tamayo, P., Mootha, V.K., Mukherjee, S., Ebert, B.L., Gillette, M.A., Paulovich, A., Pomeroy, S.L., Golub, T.R., Lander, E.S., and Mesirov, J.P. (2005). Gene set enrichment analysis: a knowledge-based approach for interpreting genome-wide expression profiles. Proc Natl Acad Sci U S A *102*, 15545-15550. 10.1073/pnas.0506580102.
72. Yu, G., Wang, L.G., Han, Y., and He, Q.Y. (2012). clusterProfiler: an R package for comparing biological themes among gene clusters. OMICS *16*, 284-287. 10.1089/omi.2011.0118.
73. Walter, W., Sanchez-Cabo, F., and Ricote, M. (2015). GOplot: an R package for visually combining expression data with functional analysis. Bioinformatics *31*, 2912-2914. 10.1093/bioinformatics/btv300.

Table 1. Aberrant phenotypes in sh*Dmrt2* and mock electroporated brains at E18.5.

	Male Mock	**Male sh*Dmrt2***	**Female Mock**	**Female sh*Dmrt2***
IUE GFP(+) area (μm^2)	40.16 ± 2.08	30.48 ± 4.28	41.70 ± 0.72	46.02 ± 2.87
IUE GFP(+) fluorescence intensity (au) [(a)]	130.84 ± 9.00	83.54 ± 10.31	143.98 ± 18.04	126.13 ± 8.27
GFP(+) gaps [(b)]	No	Yes	No	Yes
Migratory defect [(c)]	No	3.93 ± 1.25	No	14.46 ± 3.98
Defasciculation	No	Yes	No	Yes
VZ GFP(+) cells	Yes	No	Yes	No

[(a)] Fluorescence intensity of the electroporated area (**Figure 2A-D**) was measured by Integrated Density (area x mean gray value).
[(b)] All gaps are located at the medial cingulate cortex.
[(c)] Number of cells found at the corpus callosum.

Figure 1

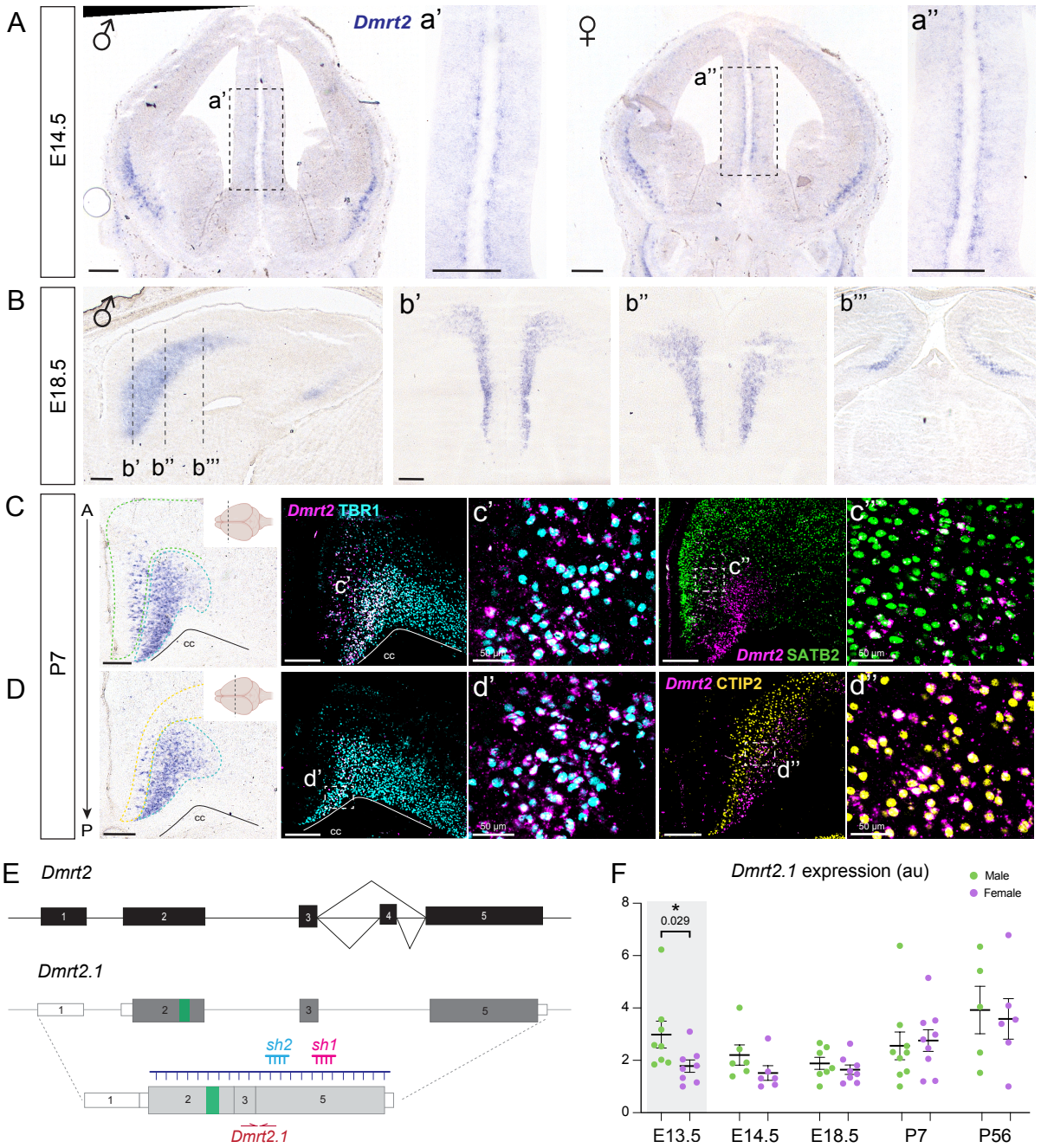

A
E14.5
Dmrt2
a'
a''
B
E18.5
b'
b''
b'''
C
D
P7
A
P
Dmrt2 TBR1
c'
c''
Dmrt2 SATB2
d'
d''
Dmrt2 CTIP2
cc
50 µm
E
Dmrt2
Dmrt2.1
sh2
sh1
F
Dmrt2.1 expression (au)
Male
Female
0.029
E13.5
E14.5
E18.5
P7
P56

Figure 2

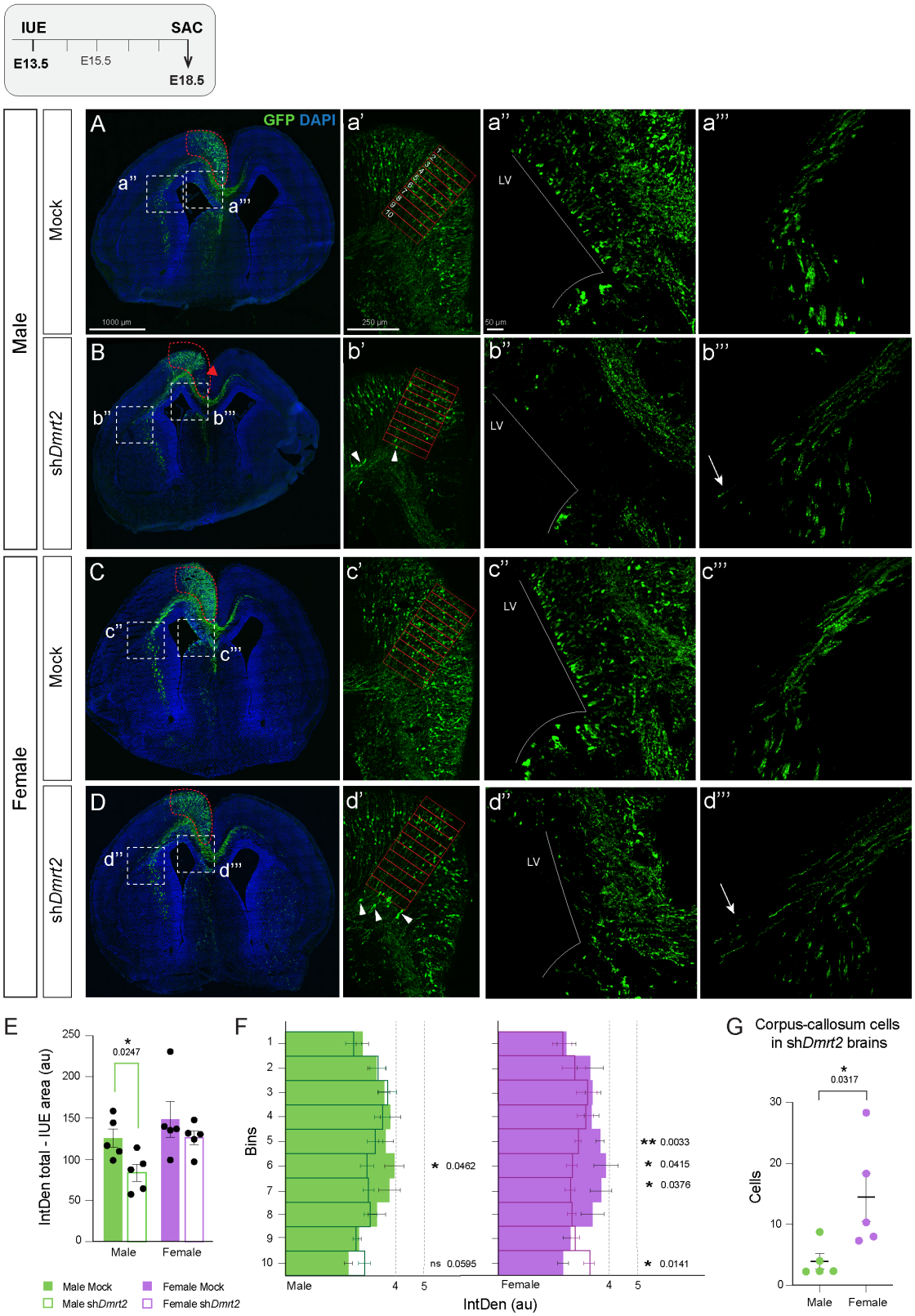
IUE
SAC
E13.5
E15.5
E18.5
Male
Female
Mock
shDmrt2
GFP DAPI
LV
1000 µm
250 µm
50 µm
E
IntDen total - IUE area (au)
0.0247
Male
Female
Male Mock
Male shDmrt2
Female Mock
Female shDmrt2
F
Bins
IntDen (au)
0.0462
ns 0.0595
0.0033
0.0415
0.0376
0.0141
G
Corpus-callosum cells in shDmrt2 brains
Cells
0.0317

Figure 3

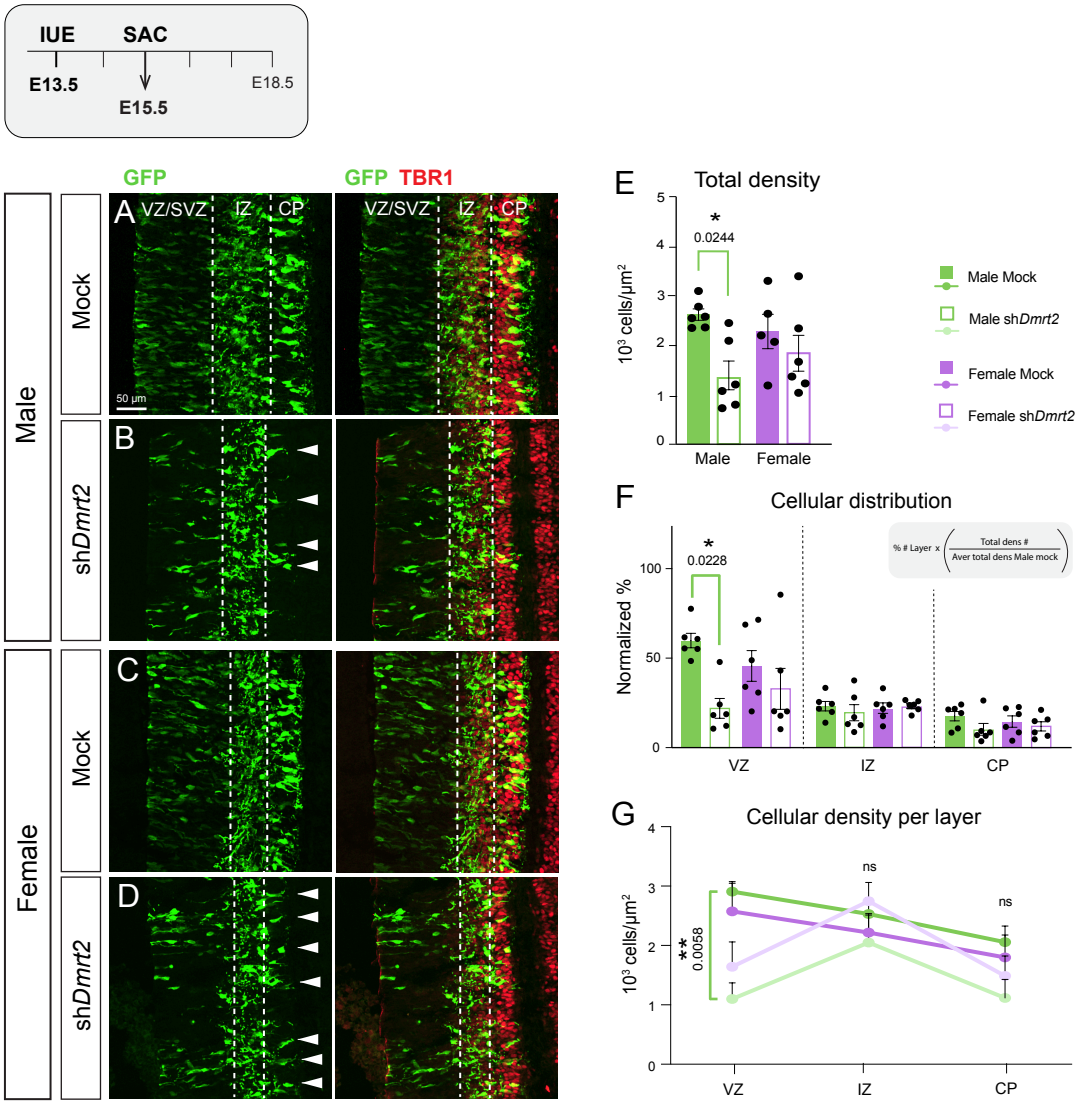
IUE
SAC
E13.5
E15.5
E18.5
GFP
GFP TBR1
Male
Female
Mock
shDmrt2
A
B
C
D
VZ/SVZ
IZ
CP
50 µm
E
Total density
*
0.0244
10³ cells/µm²
Male
Female
Male Mock
Male shDmrt2
Female Mock
Female shDmrt2
F
Cellular distribution
*
0.0228
Normalized %
VZ
IZ
CP
G
Cellular density per layer
**
0.0058
ns
ns

Figure 4

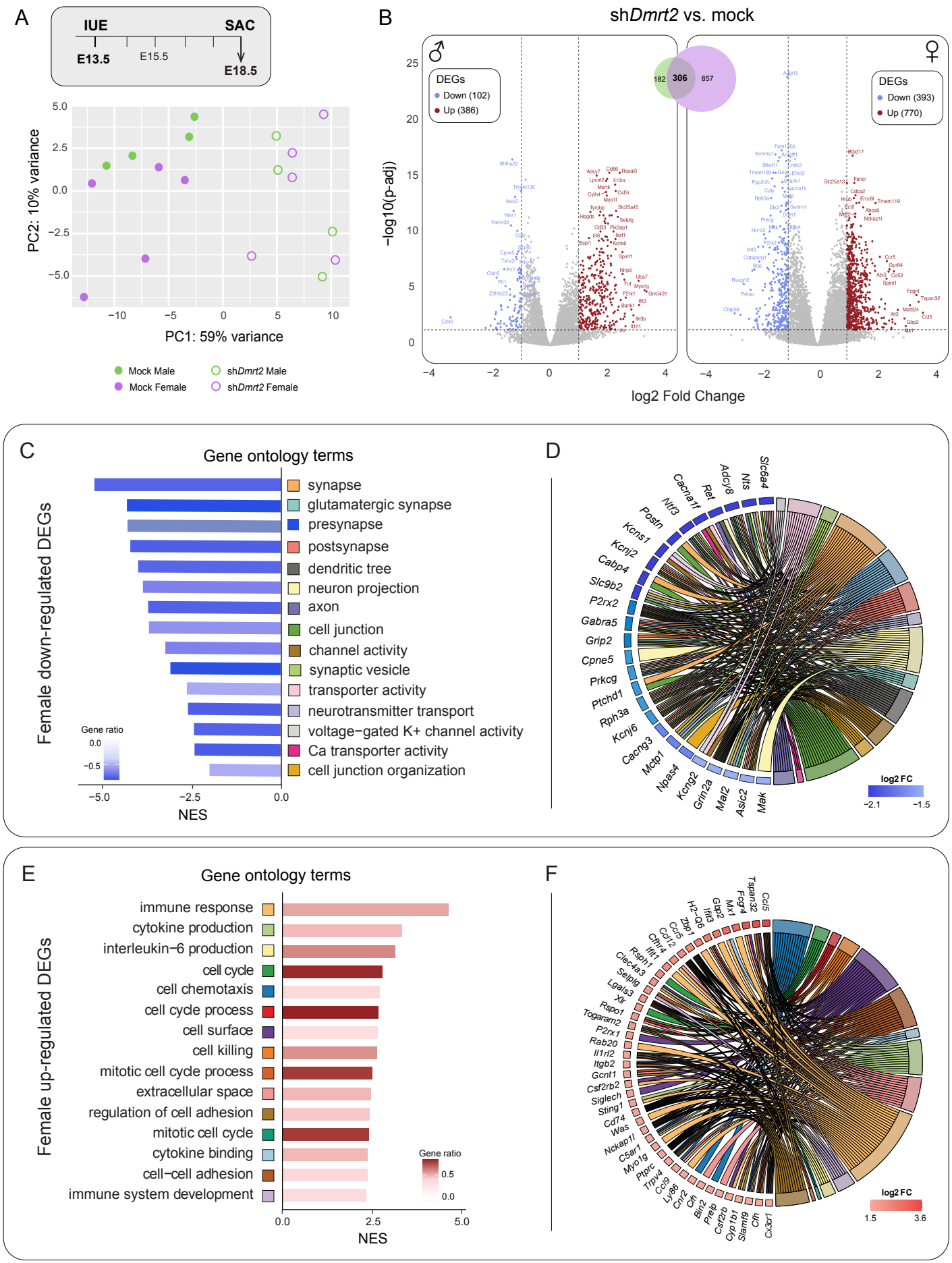
A
IUE
SAC
E13.5
E15.5
E18.5
PC2: 10% variance
PC1: 59% variance
Mock Male
Mock Female
shDmrt2 Male
shDmrt2 Female
B
shDmrt2 vs. mock
♂
♀
DEGs
Down (102)
Up (386)
182
306
857
Down (393)
Up (770)
−log10(p-adj)
log2 Fold Change
C
Gene ontology terms
Female down-regulated DEGs
synapse
glutamatergic synapse
presynapse
postsynapse
dendritic tree
neuron projection
axon
cell junction
channel activity
synaptic vesicle
transporter activity
neurotransmitter transport
voltage−gated K+ channel activity
Ca transporter activity
cell junction organization
Gene ratio
NES
D
Slc6a4
Nts
Adcyap1
Ret
Cacna1f
Ntf3
Postn
Kcns1
Kcnj2
Cabp4
Slc9b2
P2rx2
Gabra5
Grip2
Cpne5
Prkcg
Ptchd1
Rph3a
Kcnj6
Cacng3
Mctp1
Npas4
Kcng2
Grin2a
Mal2
Asic2
Mak
log2 FC
E
Gene ontology terms
Female up-regulated DEGs
immune response
cytokine production
interleukin−6 production
cell cycle
cell chemotaxis
cell cycle process
cell surface
cell killing
mitotic cell cycle process
extracellular space
regulation of cell adhesion
mitotic cell cycle
cytokine binding
cell−cell adhesion
immune system development
Gene ratio
NES
F
Ccl5
Tspan32
Fcgr4
Mx1
Gbp2
Ifit3
H2−Q6
Zbp1
Ccr5
Ccr2
Cfhr4
Ifit1
Rsph1
Clec4a3
Selplg
Lgals3
Xlr
Rspo1
Togaram2
P2rx1
Rab20
Il1rl2
Itgb2
Gcnt1
Csf2rb2
Siglech
Sting1
Cd74
Was
Nckap1l
C5ar1
Myo1g
Ptprc
Trpv4
Ccl9
Ly86
Cnr2
Cfh
Bin2
Prelp
Csf2rb
Cyp1b1
Slamf9
Cfh
Cx3cr1
log2 FC

Supplementary table 1. Aberrant phenotypes in male brains of sh*Dmrt2* and mock electroporated samples at E18.5.

Male Mock							
	S83	**S84**	**S97**	**S195**	**S199**		**Mean ± SEM**
IUE GFP(+) area (μm^2)	36.43	42.50	40.23	35.08	46.56		40.16 ± 2.08
IUE GFP(+) fluorescence intensity (au) [(a)]	125.47	144.25	109.55	116.58	158.34		130.84 ± 9.00
GFP gaps [(b)]	|	|	|	|	|		No
Migratory defect [(c)]	|	|	|	|	|		No
Defasciculation	|	|	|	|	|		No
VZ GFP(+) cells	++	++	+	+++	+++		Yes
Male sh*Dmrt2*							
	S90	**S100**	**S102**	**S164**	**S165**		**Mean ± SEM**
IUE GFP(+) area (μm^2)	37.93	16.87	24.29	34.29	39		30.48 ± 4.28
IUE GFP(+) fluorescence intensity (au) [(a)]	94.55	57.44	64.21	87.36	114.12		83.54 ± 10.31
GFP gaps [(b)]	++	+	++	+	++		Yes
Migratory defect [(c)]	2.25	2.33	4.00	2.33	8.75		3.93 ± 1.25
Defasciculation	+++	++	++	+++	+++		Yes
VZ GFP(+) cells	- - -	- - -	- -	- - -	- -		No

[(a)] Fluorescence intensity of the electroporated area (**Figure 2A-D**) was measured by Integrated Density (area x mean gray value).
[(b)] All gaps are located at the medial cingulate cortex.
[(c)] Number of cells found at the corpus callosum.
(|) No phenotype
(+) Ectopic cells or branching (color intensity increases with phenotype)
(-) Absence of cells (color intensity increases with phenotype)

Supplementary table 2. Aberrant phenotypes in female brains of sh*Dmrt2* and mock electroporated samples at E18.5.

Female Mock							
	S86	**S98**	**S99**	**S198**	**S200**		**Mean ± SEM**
IUE GFP(+) area (μm^2)	40.56	41.85	44.42	40.56	41.09		41.70 ± 0.72
IUE GFP(+) fluorescence intensity (au) [(a)]	99.07	209.82	135.11	139.64	136.24		143.98 ± 18.04
GFP gaps [(b)]	|	|	|	|	|		No
Migratory defect [(c)]	+	|	+	|	|		No
Defasciculation	|	|	|	|	|		No
VZ GFP(+) cells	+++	+	+++	+++	+++		Yes
Female sh*Dmrt2*							
	S89	**S93**	**S166**	**S167**	**S168**		**Mean ± SEM**
IUE GFP(+) area (μm^2)	50.91	45.89	40.47	53.82	38.99		46.02 ± 2.87
IUE GFP(+) fluorescence intensity (au) [(a)]	131.63	96.90	147.66	130.22	124.26		126.13 ± 8.27
GFP gaps [(b)]	+	++	+	+	+		Yes
Migratory defect [(c)]	8.00	7.33	28.33	10.33	18.33		14.46 ± 3.98
Defasciculation	+++	+++	+	++	+++		Yes
VZ GFP(+) cells	- - -	- - -	- -	- - -	- - -		No

[(a)] Fluorescence intensity of the electroporated area (**Figure 2A-D**) was measured by Integrated Density (area x mean gray value).
[(b)] All gaps are located at the medial cingulate cortex.
[(c)] Number of cells found at the corpus callosum.
(|) No phenotype
(+) Ectopic cells or branching (color intensity increases with phenotype)
(-) Absence of cells (color intensity increases with phenotype)

Suppl Figure 1

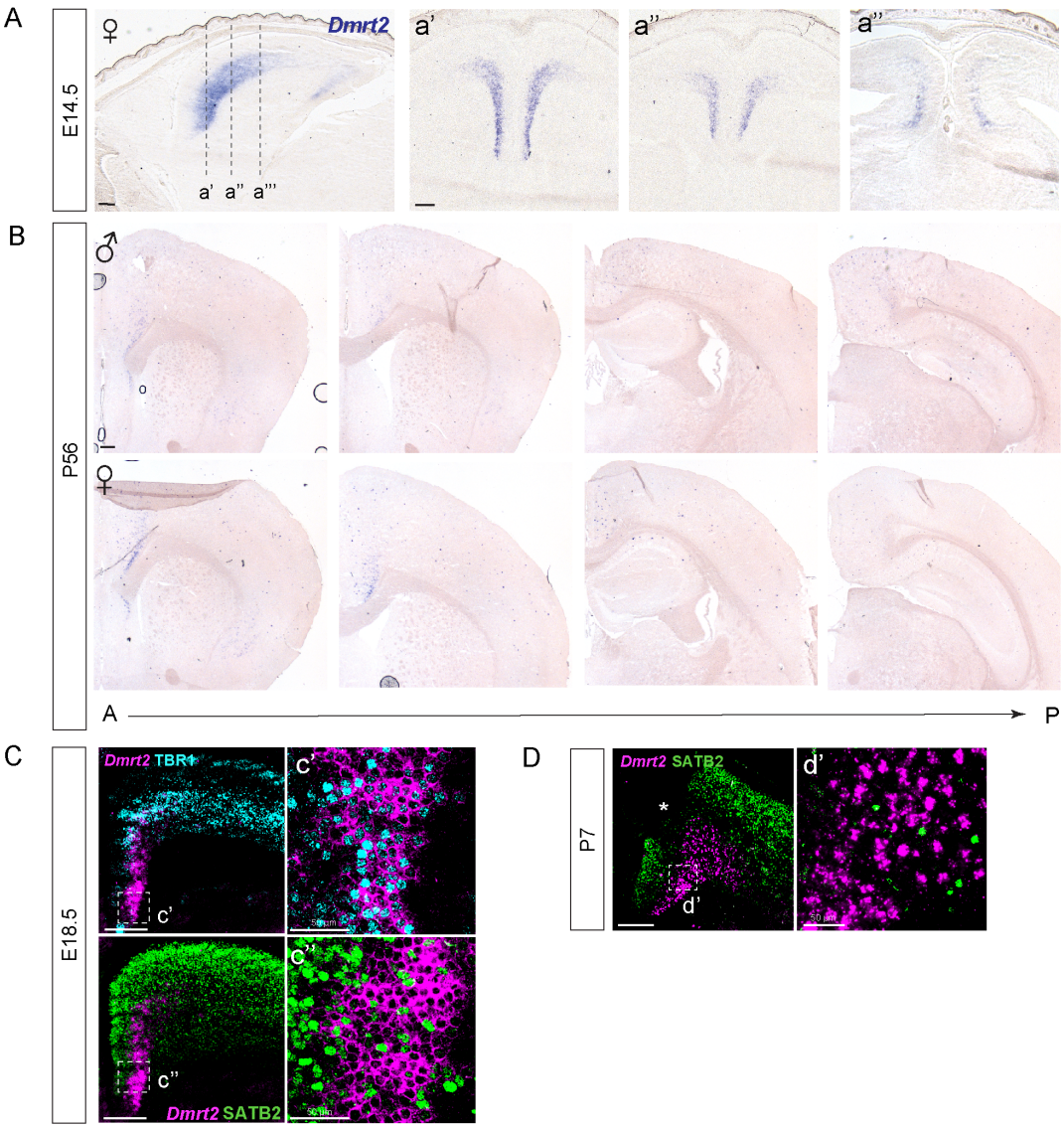

Supplemental Figure 2

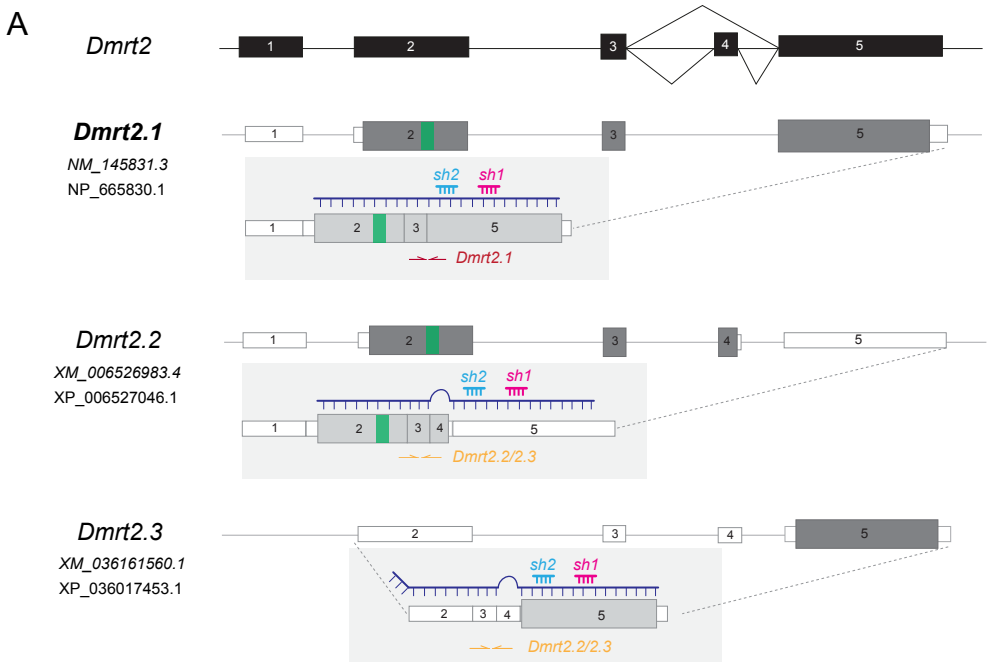

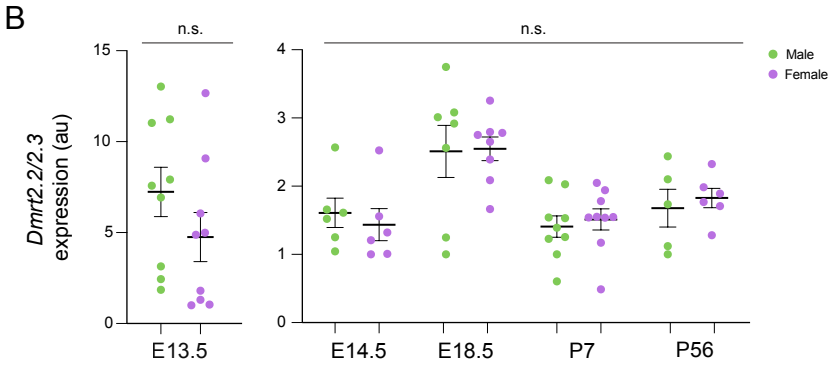

Suppl Figure 3

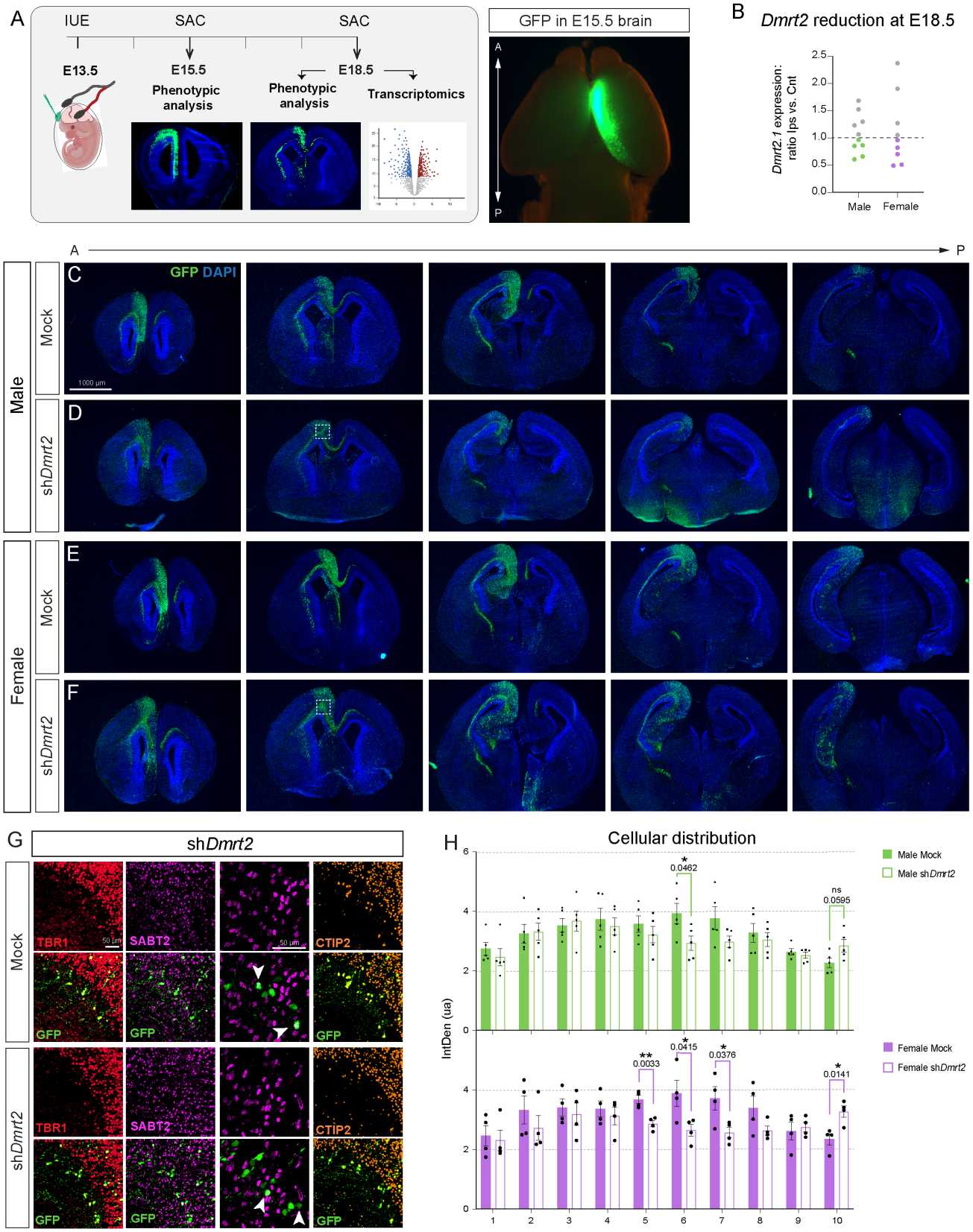

Suppl Figure 4

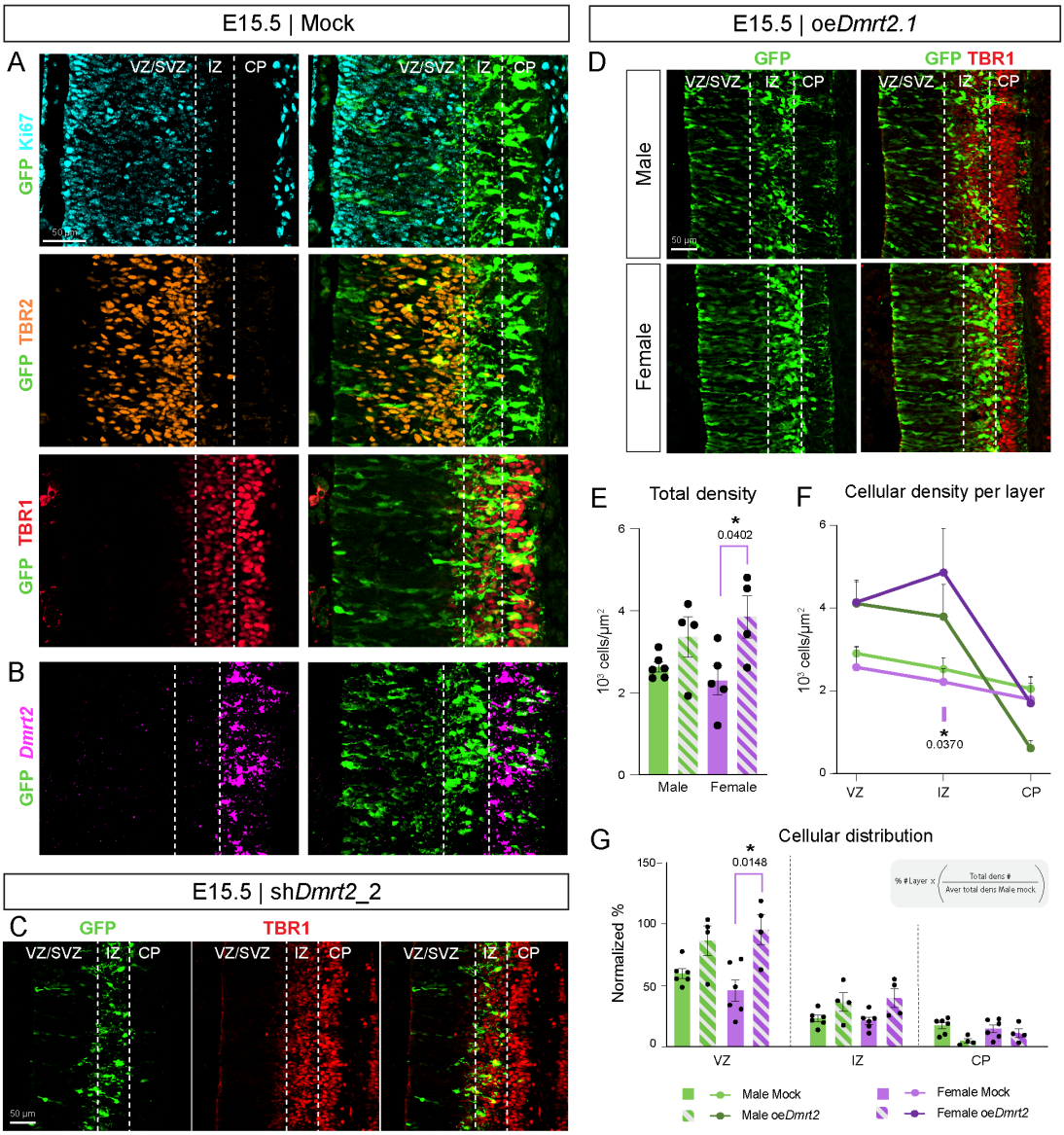

H

	Cellular distribution (%)						Cellular density (10^3 cells/µm^2)					
	VZ/SVZ		IZ		CP		VZ/SVZ		IZ		CP	
	Mean	±SEM	Mean	±SEM	Mean	±SEM	Mean	±SEM	Mean	±SEM	Mean	±SEM
Male mock	59.84	4.04	23.06	2.64	17.11	2.63	2.91	0.17	2.53	0.28	2.06	0.27
Male sh*Dmrt2*	21.95	5.55	19.41	4.51	9.76	3.32	1.10	0.27	2.05	0.47	1.12	0.31
Male oe*Dmrt2.1*	86.36	12.01	36.47	7.58	4.83	1.79	4.12	0.57	3.80	0.77	0.62	0.20
Female mock	45.68	8.59	21.27	2.91	14.59	3.15	2.57	0.47	2.22	0.32	1.80	0.38
Female sh*Dmrt2*	32.88	11.44	22.46	1.30	11.92	2.58	1.64	0.42	2.75	0.32	1.49	0.34
Female oe*Dmrt2.1*	95.49	12.05	39.60	7.64	11.06	3.61	4.15	0.49	4.86	1.07	1.70	0.66
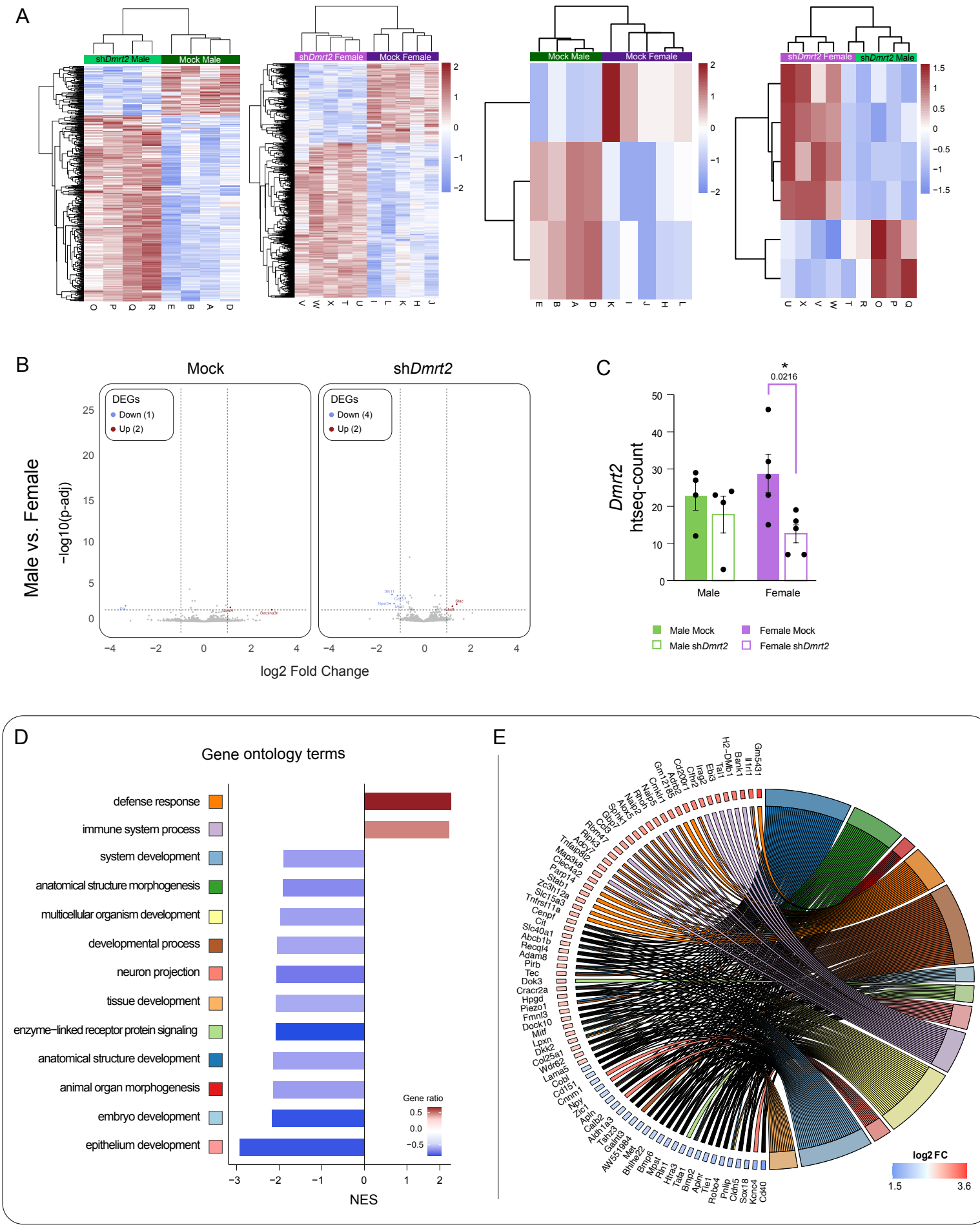
Supplemental Figure 5